SHOCK ADIABATIC CURVES OF METALS.

NEW DATA, STATISTICAL ANALYSIS, AND GENERAL LAWS

L. V. Al'tshuler, A. A. Bakanova,*
I. P. Dudoladov, E. A. Dynin,
R. F. Trunin, and B. S. Chekin

UDC 532.593+536.715:546.3

1. Experimental Investigation and Classification of the Hugoniot Adiabatic Curves

Shock-wave methods [1-3], based on the recording of the kinematic parameters of the wave (the velocity D of the motion of its wave front and the velocity u of the substance), uniquely determine the thermodynamic characteristics of substances at pressures of tens or hundreds of gigapascals (1 GPa = 10 kbar). The Hugoniot adiabatic equations so obtained, which are known today with different degrees of accuracy and in different ranges for almost all metallic elements, are widely used for constructing semiempirical equations of state [1-4]. Referred to briefly as D—u relations, they also convert each substance under study into a tensometer of the dynamic and static pressures [5] in the megabar range. The effectiveness of using the results of dynamic investigations for all these purposes is determined by the amount of original experimental information available and by the dimensions of the investigated region of the phase plane.

The authors present below some new data characterizing the dynamic compressibility of 26 elements. For six metals (Ti, Ta, Mo, Ce, Gd, and Ge) the thermodynamic parameters (pressure $p=\rho_0 uD$ and degree of compression $\delta=\rho/\rho_0$) are shown together with the values of D and u in Table 1, determined at maximum pressures in the laboratory experiment. These results were obtained when iron strikers impelled by detonation products to velocities close to 15 km/sec (for iron the velocity exceeded 19 km/sec) collided with targets. The measurements made extended the experimental interval of pressures for Fe by a factor of 1.5, i.e., up to 1340 GPa, and for Ti, Mo, Ce, and Gd by a factor of about 2. The reduced data determined the positions of the adiabatic curves at the new level of pressure and, in addition, provided more accurate information on the slopes of the compression curves at the boundaries of previously investigated intervals. The new points are indicated by a numeral 1 on the D—u diagrams of Figs. 1-3 and, on a logarithmic scale of variation of the pressures and deformations, $z=1-\delta^{-1}=u/D$, for Mo, Fe, and Pb in Fig. 4. There is satisfactory agreement between the Mo points for 1000 GPa and the states behind the shock-wave front of a strong underground explosion at pressures which are twice as high [6] (these are indicated by a plus sign, taking account of the experimental errors, in Figs. 1 and 4).

In Table 2, we show for eight elements the values of D and u obtained at striker velocities of up to 9 km/sec (for Sn up to 14 km/sec), and in Table 3 we show the experimental results for 10 elements in the same striker velocity range; these values had been previously represented only graphically in [7]. This table also includes data on Ag and Au, determined more accurately by a comparison with the original source [8] and supplemented by new points for Ag.

TABLE 1

Element	ρ_0, g/cm³	u, km/sec	D, km/sec	p, GPa	δ
Ce	6,75	7,26	11,39	558	2,758
Gd	7,93	7,02	10,73	597	2,892
Ti	4,50	9,26	15,14	631	2,575
Ta	16,38	5,86	11,00	1055	2,140
Mo	10,20	6,59	13,55	910	1,947
Mo	10,20	7,05	14,06	1011	2,006
Fe	7,85	9,70	17,74	1350	2,206

*Deceased.

Moscow. Translated from Zhurnal Prikladnoi Mekhaniki i Tekhnicheskoi Fiziki, No. 2, pp. 3-34, March-April, 1981. Original article submitted March 10, 1980.

0021-8944/81/2202-0145$07.50

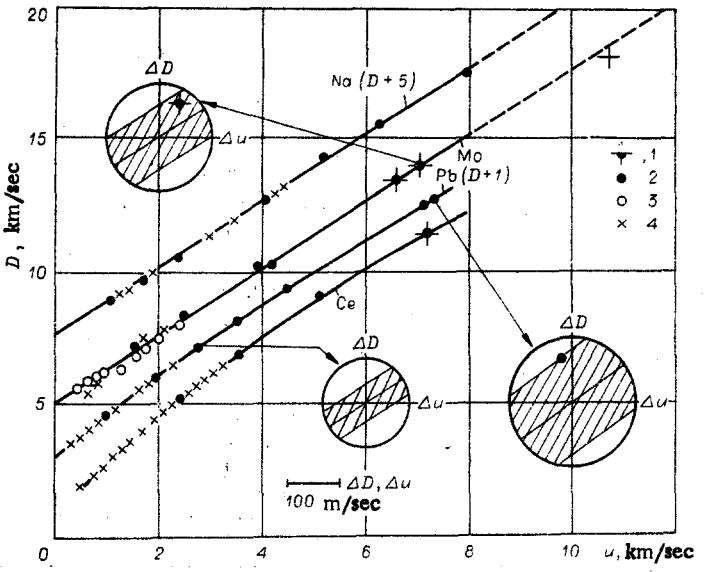

Fig. 1

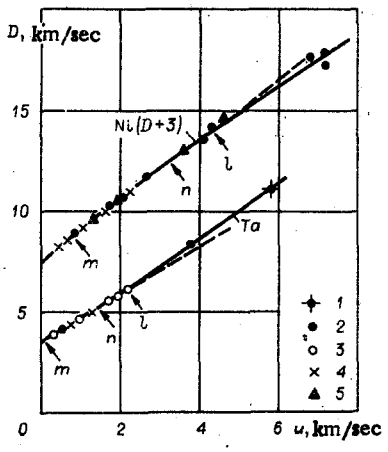

Fig. 2

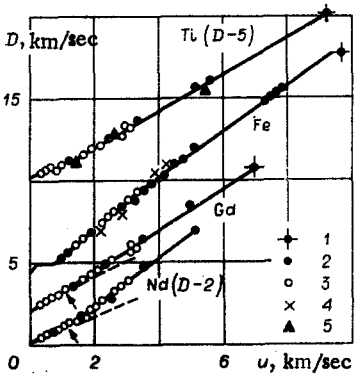

Fig. 3

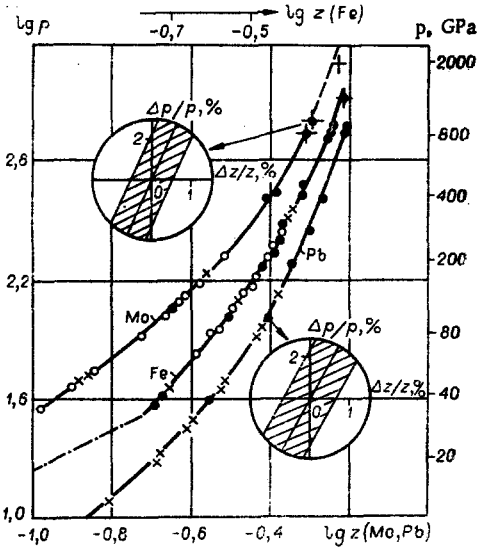

Fig. 4

TABLE 2

u, km/sec	D, km/sec	u, km/sec	D, km/sec	u, km/sec	D, km/sec
Al, ρ_0=2,71 $\frac{g}{cm^3}$		Cu, ρ_0=8,93 $\frac{g}{cm^3}$		0,52	5,08
0,86	6,52	0,175	4,15	0,71	5,22
1,24	7,08	0,350	4,39	Zn, ρ_0=7,14 $\frac{g}{cm^3}$	
1,38	7,28	0,430	4,53	3,01	7,90
2,03	8,05	0,590	4,73	3,29	8,07
2,72	8,99	0,735	5,09	3,78	8,85
3,27	9,67	0,845	5,17	Cd, ρ_0=8,64 $\frac{g}{cm^3}$	
3,30	9,88	1,27	5,80	3,15	7,15
3,72	10,30	1,75	6,52	3,63	8,13
Mg, ρ_0=1,74 $\frac{g}{cm^3}$		Ni, ρ_0=8,87 $\frac{g}{cm^3}$		3,71	8,21
1,41	6,28	0,91	5,91	Sn, ρ_0=7,28 $\frac{g}{cm^3}$	
1,85	6,77	1,98	7,61	3,34	7,59
3,27	8,51	4,07	10,60	3,86	8,23
3,99	9,37	Nb, ρ_0=8,58 $\frac{g}{cm^3}$		3,93	8,28
4,99	10,10	0,40	4,94	7,71	12,57

For calculating the equations of the adiabatic curves of metallic elements and obtaining a realistic estimate of the errors, we performed a statistical analysis of the results of wave measurements on metals carried out in the USSR and abroad up to 1977. On the basis of methodological criteria, all the original information on the dynamic compressibility was divided into three groups:

a) The data of shock-wave measurements [8-19] and Tables 1-3 were obtained in the Soviet Union by the most-rigorous deceleration method [9, 1], when the mass velocity u is found from the velocity of motion of the striker before it collides with the target made of the substance under study. These experiments, performed at substantially different shock-wave amplitudes, established the shock compression state of 44 metals up to pressures of 400-1300 GPa. It should be noted that in our further processing we did not make direct use of the compressibility characteristics published in [8, 9], since the corrected data for these studies are found in [10] for Fe, Pb, and Cu, in [11] for Zn, Cd, and Sn, and in Table 3 of the present study for Au and Ag. For Al, Cu, Fe, and Pb the earlier experiments (except for [13]) were generalized and supplemented in [20]. In all the studies of group "a" the D–u point is obtained by averaging four to six experiments.

b) The results of the individual measurements by the deceleration method were carried out on pneumatic apparatus for Au and W [21], Pt [22], Be, Ti, Ni, Cu, and Al [23], and using accelerated explosions of strikers [24] for two metals used as standards (Cu and Fe) and 16 other elements. Group "b" also includes data [25-27] on the investigation of rare-earth metals, in which the "screens" used in the impedance method (the reflection method) were metals previously studied independently [24].

c) Investigations were carried out in which the values of D and u for each point on the Hugoniot adiabatic curves was obtained in individual measurements and which are founded on less-rigorous determinations of the mass velocities on the basis of the velocity of motion of the free surface of the specimen or the standard substance. This group of studies includes investigations of the compressibility of 27 metals up to 50 GPa [28], 19 metals up to 150-200 GPa [29], alkali metals up to 40 GPa [30], and the reports published in [31], showing no systematic deviation from the most important publications, for a number of metals in the range 40-150 GPa; this group also includes the data of [32], found by the deceleration method but showing a large experimental dispersion and included in the processing only for Mg and Fe.

The properties of metals at high pressures are interpreted by the authors within the framework of the hydrodynamic model, which is rigorously applicable above shock-melting pressures. However, in accordance

TABLE 3

u, km/sec	D, km/sec	u, km/sec	D, km/sec	u, km/sec	D, km/sec
Ga, ρ_0=5,91 $\frac{g}{cm^3}$		Co, ρ_0=8,30 $\frac{g}{cm^3}$		Ho, ρ_0=8,73 $\frac{g}{cm^3}$	
0,635	3,46	1,77	7,07	0,57	2,84
1,305	4,63	2,93	8,92	1,24	3,44
2,38	6,15	4,32	11,13	2,25	4,60
5,10	10,46	Rh, ρ_0=12,4 $\frac{g}{cm^3}$		3,30	6,10
In, ρ_0=7,29 $\frac{g}{cm^3}$		0,31	5,01	4,82	8,34
0,56	3,50	0,74	5,71	Au, ρ_0=19,3 $\frac{g}{cm^3}$	
1,19	4,36	1,45	6,90	0,71	4,27
2,18	5,90	3,80	10,55	1,72	5,74
4,87	7,75	Ir, ρ_0=22,65 $\frac{g}{cm^3}$		3,25	8,16
Tl, ρ_0=11,86 $\frac{g}{cm^3}$		0,23	4,26	Ag, ρ_0=10,49 $\frac{g}{cm^3}$	
4,32	8,26	0,54	4,84	0,93	4,69
Cr, ρ_0=7,18 $\frac{g}{cm^3}$		1,10	5,67	1,75	6,10
4,62	11,42	3,09	8,82	2,13	6,76
Re, ρ_0=21,03 $\frac{g}{cm^3}$		Pr, ρ_0=6,81 $\frac{g}{cm^3}$		2,63	7,56
0,23	4,41	0,68	2,63	3,98	9,48
0,57	4,77	1,42	3,36	4,32	9,73
1,15	5,68	2,48	4,95		
3,26	8,55	5,12	9,08		

with the experiments carried out on tungsten [33], copper, and aluminum [34], it is assumed that even for pressures ≥10 GPa the metal preserving its elastoplastic properties is in a relaxed, quasihydrostatic state behind the shock-wave front. With such an approach, the shock-wave information necessary for constructing the "hydrodynamic" adiabatic curves must be supplemented by information on the volumetric compressibility of metals under normal conditions.

d) The fourth group consists of original data on the isentropic velocity of sound c_0 at normal conditions, which were obtained by various methods: from analytic formulas describing the behavior of curves of isothermal compression [35-39], from the values of the moduli of elasticity of polycrystalline specimens under normal conditions [35], from calculations based on the velocities of ultrasonic waves along different directions of a single crystal [40, 41], and from the velocities of longitudinal and transverse waves in polycrystals [22, 24, 26, 27, 39].

The main types of adiabatic curves, differing in the approximation method used, are shown in the D–u diagrams of Figs. 1-3, using the examples of metals of Table 1 and also Na, Pb, Ni, and Nd, by smooth or piecewise-smooth curves having constant or slowly varying slopes. The experiments belonging to groups "a"-"c" are indicated here by the points 2-4, respectively. The results from group "b," obtained on high-speed pneumatic systems [21-23], are indicated by the points 5, and the data of Table 1 are indicated by the points 1 (the same notation is used in Figs. 4 and 7).

Even in the first investigations [8, 9, 28], it was found that many metals had a linear relation between the velocity of the shock wave and the mass velocity of the substance. For the lower segments of the adiabatic curves, which in metals with low compressibility included pressures of several hundred gigapascals, this relation, determined mainly by the "cold" interaction of atoms, is the predominant one. There is no rigorous justification for the linearity of the D–u relations. It is confirmed, to a certain extent, by calculations using model potentials, which were performed in [42, 43] for Na, KI, and CsI.

As the amplitude of the shock waves increases, the thermal components of the total energy and the total pressure of the shock compression of the metals increase progressively [1-3]. The limiting value of the derivative D'_u for large amplitudes is found by the Thomas–Fermi theory and is represented by the value $D'_{u\infty} \approx 1.25$ [44]. The configurations of the adiabatic curves which have no singularities are determined in the first approximation by the ratio of the initial values D'_{u0} and the asymptotic values $D'_{u\infty}$ of the derivatives. For $D'_{u0} > 1.5$ the characteristic adiabatic curves are convex curves with a markedly reduced slope for large values of u. For $D'_{u0} \approx 1.0$-1.3 the curve remains linear or deviates upward. The last form is characteristic of a number of transition metals with a high intensity of electron states and anomalously high Gruneisen electron coefficients [45].

For a wide group of elements, including some of the alkali, alkaline-earth, and transition metals and all of the rare-earth metals, investigators in the Soviet Union [16-19] and abroad [25, 27] have discovered distinctive adiabatic curves with break points separating states with high compressibility from those with low compressibility, which result from the migration of outer electrons to free inner orbits. A special group of adiabatic curves is constituted by D–u relations of stepwise form, reflecting [1-3] the existence of different crystalline forms at different pressure levels.

In the light of the systematization adopted in the scheme we describe, the adiabatic curves were divided into five fundamental types.

Adiabatic curves of type 1, an example of which is the curve for Mo (see Fig. 1), on the basis of statistical criteria for all the known values of the parameters admit of approximation by linear relations of the form

$$D = a_0 + a_1 u, \; a_0, \; a_1 > 0. \tag{1.1}$$

Parabolic adiabatic curves of type 2, given by the equations

$$D = a_0 + a_1 u + a_2 u^2, \; a_0, \; a_1 > 0, \; a_2 < 0, \tag{1.2}$$

are represented by the compression curves of Pb and Ce (see Fig. 1).

Adiabatic curves of type 3 correspond to Eq. (1.2) but with a coefficient $a_2 > 0$, for example Na in Fig. 1.

In a number of type-2 and type-3 metals within the significant portion of the investigated range, it is statistically better justified to use an alternate linear approximation. Such adiabatic curves, belonging to type-2* or type-3*, are shown in Fig. 2 for Ni and Ta. Within the linear interval, for $u \leq u_l$, the approximating straight lines practically coincide with the parabolas, intersecting them at the points m and n. For $u > u_l$, where the straight lines are given in dashed form, the difference becomes significant and the linear description is not applicable.

Adiabatic curves of type 4, which have break-points (indicated by an arrow in Fig. 3 for Gd and Nd) result from the formation of electron configurations which have low compressibility under pressure. Here the lower branches are always straight lines, while the upper segments are represented by Eq. (1.1) or Eq. (1.2) with positive or negative coefficients a_2.

The D–u relations of stepwise form (type 5) occur in the case of polymorphic transitions of the first kind or the case of anomalous melting. This type of D–u diagram is found, in particular, in the case of Fe and Ti (Fig. 3). In the systematization we have adopted, we can use Eq. (1.1) or Eq. (1.2) for approximating the upper branches. A more exact analytic form of the D–u curves, adequately representing the specifics of the phase transition, was found in [4], for the case of iron (shown below).

The smoothness of the approximating curves does not justify the conclusion that the substance has no electron or phase transitions. Such transitions may take place at pressures lower than in the dynamic experiments, or they may be accompanied by a small change in density and compressibility. The corresponding adiabatic curves (depending on their configuration) can naturally be "attributed" to one of the types 1-3, but the question of the inclusion of the values of c_0 in the approximated data field required a special analysis.

For this purpose, we performed test calculations which did not take account of the values of c_0. If the nominal values of a_0 so obtained differed substantially from c_0 on the low side, in comparison with the characteristic errors, this provided a proof, independent of the statistical investigations, that a transition did exist. With most of the substances investigated, for a more exact description of the hydrodynamic adiabatic curves, at low values of u, it was found possible to include the experimental values of c_0 in the final variant of the processing according to the method described below (data of group "d").

The extensive experimental material taken together enables us to find the most reliable analytic functions for the adiabatic curves of the metals and, on the basis of the statistical analysis, to determine the degree of accuracy of their positions in the field of kinematic and thermodynamic variables.

Simultaneous processing of shock-wave measurements from different sources had been carried out earlier as well, for example, in [23] and [29] in terms of the D–u variables, in [4] in terms of p–z variables which had not been directly measured, and also in [13] and many other studies in which the equations of state were constructed. In addition to providing new information and expanding the ranges of values, the approach we have developed differs from others in using statistical criteria and in the calculation of the accuracy of the characteristics, including the accuracy of the localization of the break points.

It should be noted that the "errors" in the values of D mentioned in [29] show how close the nominal curves come to the experimental points; they have no statistical meaning with respect to the unknown true functions D(u). At the same time, the "confidence intervals" [47, 48] determined here provide a probable estimate for the degree of closeness of the nominal and true adiabatic curves.

In order to illustrate the use of the methods developed below, in Fig. 1, for the adiabatic curves of Mo and Pb, the enlarged-scale insets show the confidence intervals indicated by shading. Unlike the values of a_k, D(u) for their functions – p, z, etc. – the method used here does not permit us to calculate rigorously the form of the distribution functions and the confidence intervals, but the error estimates needed for practical use can be obtained from the theory of error transfer [49]. In insets in Fig. 4 the elements of the band of indeterminacy of the dynamic-compression curves in the variables log p and log z are shaded, shown at a magnification of 23, for Mo at 1000 GPa and Pb at 100 GPa.

2. Principles of Statistical Processing of the D – u Relations for 32 Elements

The purpose of a statistical analysis of the experimental data on smooth D–u relations of types 1, 2, 3, 2*, and 3* is to ascertain the "nominal," i.e., the most reliable D–u equation of the adiabatic curves and to obtain probability estimates for the deviations of the nominal wave velocities and regression coefficients in Eqs. (1.1) and (1.2) from the true values. The possible errors in the nominal values are due to individual errors in the measurements of the two kinematic parameters D and u.

However, in the regression method used below there is only one "reduced" error σ_i, corresponding to the deviation of D for fixed u. If the results of the measurements of D_i and u_i are independent, involve no systematic errors, and are characterized by their errors $\Delta_i D$ and $\Delta_i u$, then

$$\sigma_i \approx [(\Delta_i D)^2 + (D'\Delta_i u)^2]^{1/2} = D_i\left[\left(\frac{\Delta_i D}{D}\right)^2 + \left(zD'\frac{\Delta_i u}{u}\right)^2\right]^{1/2}. \qquad (2.1)$$

It is convenient to assume that the values of D_i and u_i included in the processing correspond to the i-th experiment, in which u_i is fixed while the value of D_i is distributed according to a normal law with variance σ_i. Such a simplifying assumption enables us to use the method of least squares [47-49] if we can obtain specific values for the ratio of the quantities σ_i in different experiments.

We assume that $\sigma_i/(D_i\sqrt{g_i}) = \text{const}$, where g_i is a coefficient depending on the method of investigation and, in addition, is proportional to a number of experiments in the series [47] if as the pair of values D, u we use the results obtained by averaging the series of experiments. Thus, for sources in group "a" we selected g = 4; for group "b," taking account of the accuracy of the method, we selected g = 2; and for group "c" we selected g = 1. The data of group "d" were regarded as values of $D_i(0)$, and when they were included in the calculations, we assumed for these that g = 1.

According to the formula adopted, for identical values of g we have $\sigma_i/D = \text{const}$, i.e., the reduced relative errors of the measurement of the wave velocities were assumed to be constant. The values of D and u, which are of the same type, are usually measured with relative errors which are close to each other ($\Delta_i D/D \approx \Delta_i u/u_i$ and $(zD'_u)^2 \leq 1$). If, taking account of these facts, we disregard the second term on the right side of (2.1), the condition $\sigma_i \sim D_i$ is equivalent to the condition that we have a constant relative error in the recording of the time motion of the wave T_i, since $D_i = L_i/T_i$, and the base line L_i is determined with a high degree of accuracy.

For our further analysis, we introduce the concept of the confidence interval $\Delta_A(q)$ of a statistically distributed quantity A for a level of probability q. We assume that the quantity A is symmetrically distributed about its mean value A* and $\Delta_A(q)$ is determined on the basis of the fact that the inequality $|A - A^*(q)| < \Delta_A(q)$

is satisfied with the indicated probability. For example, in the case of a normal distribution, we know with probability 0.68 that the deviation from the mean does not exceed the variance, i.e., the confidence interval indicated for q = 0.68 by Δ_A^0 coincides with the variance.

The parameters a_k introduced in (1.1), (1.2) and the function D(u) for fixed u are determined from random values of D_i and u_i, and therefore, they are also random values; however, they are subject to a distribution law more complicated than the normal law. Nevertheless, it is natural, by analogy, to assign the meaning of errors to quantities $\Delta_{a_k}^0$ and Δ_D^0, which constitute the corresponding confidence intervals for q = 0.68.

The general scheme for smoothing the measurements by means of a polynomial has been described in the literature [47-49], and therefore the overall formulas will be given here only for the simplest variant of the linear regression (1.1). In the general case the form

$$M(a_k) = \sum_{i=1}^{n} W_i [D_i - D(u_i)]^2 \Big/ \sum_{i=1}^{n} W_i \tag{2.2}$$

takes on a minimum value for the most probable values of a_k, denoted by a_k^*, where the number n of points included in the calculation must be considerably larger than the number of parameters of the function D(u), and the statistical weight $W_i \sim \sigma_i^{-2}$.

Introducing for any function X of the observed quantities the notation $\langle X \rangle = \sum_{i=1}^{n} W_i X_i \Big/ \sum_{i=1}^{n} W_i$, we represent the nominal coefficients and the confidence intervals for type-1 adiabatic curves by the expressions

$$a_1^* = \frac{\langle Du \rangle - \langle D \rangle \langle u \rangle}{\langle u^2 \rangle - \langle u \rangle^2}, \quad a_0^* = \langle D \rangle - a_1^* \langle u \rangle; \tag{2.3}$$

$$\Delta_{a_1}(q) = \frac{M(a_0^*, a_1^*)\, t_{n-2}(q)}{\sqrt{(n-2)(\langle u^2 \rangle - \langle u \rangle^2)}}; \tag{2.4}$$

$$\Delta_D(q) = \Delta_{a_1}(q) \left[2F_{2,n-2}(q)(u^2 - 2u\langle u \rangle + \langle u^2 \rangle)\right]^{1/2} t_{n-2}^{-1}(q). \tag{2.5}$$

The functions $t_{n-2}(q)$ and $F_{2,n-2}(q)$ are tabulated coefficients defined according to [47] for the Student and Fischer distributions, respectively, corresponding to the probability q. For sufficiently large values of n, the Student distribution closely approaches the normal distribution, and since $t_{n-2}(q) \approx 1$, it follows that the coefficient of $t_{n-2}(q)$ on the right side of (2.4) is the variance of the quantity a_1. The values of $\Delta a_0(q)$ are calculated from (2.5):

$$\Delta_{a_0}(q) = \Delta_D(q)|_{u=0}.$$

In the D–u plane the curve of the boundary of the confidence intervals for different values of u and fixed q is the envelope of a pencil of straight lines. On all of these straight lines the form M takes on the same value, and for smaller values of M the straight lines lie entirely within the confidence region. As q increases from 0.68 to 0.95 in the case of a normal distribution, $\Delta(q)$ doubles, and in the calculation according to (2.5) it becomes slightly less than twice as large (proportional to $|\ln(1-q)|$).

The properties discussed above are illustrated schematically in Fig. 5, where 1 is the nominal adiabatic curve of D(u), lines 2 and 3 are asymptotes which are tangent as $u \to \pm\infty$ to the boundaries of the confidence intervals with q = 0.68 (the dashed lines), and the dot–dash lines bound a region with half-width Δ_D (q = 0.95). For substances with a linear D–u graph the values of Δ_D^0 have a minimum $\Delta_{D\min}^0$ when $u = \langle u \rangle$, and for any values of u they can be calculated by the formula

$$\Delta_D^0 = \{[(\Delta_{D\max}^0)^2 - (\Delta_{D\min}^0)^2](u - \langle u \rangle)^2 (u_{\max} - \langle u \rangle)^{-2} + (\Delta_{D\min}^0)^2\}^{1/2},$$

where the quantities u_{max} and Δ_{Dmax}^0 are the largest practically realizable values of u and Δ_D^0 for this point.

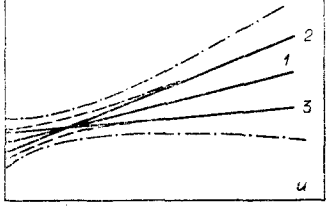

Fig. 5

The hypothesis that (1.1) is applicable was verified in the standard way [47-49], using the Fischer criterion. For a significance level of $\alpha < 10\%$, this hypothesis was rejected, and we adopted for the function D(u) a quadratic law (1.2) for which the expressions for the confidence intervals are much more complicated [47] than (2.3)-(2.5). The variation of Δ_D^0 as a function of u is characterized, as before, by a minimum within the experimental region, but this curve may also show a change in sign for the curvature and a second minimum.

We also verified the assumption that there are no systematic errors for the points included in the calculation. If this assumption were false for the groups from any source, they would have been substantially displaced in one direction from the approximating curve constructed for the majority of the more reliable data. Analysis has shown that such a situation exists in the case of the number of the studies compiled in [31], and these results were not included in the processing. In addition, we used the criterion of discarding individual observations which were conspicuously isolated from the rest [48] (the Chauvenet criterion) modified for the case of different statistical weights. The data of various authors were processed jointly if the initial densities of the specimens they used differed from the normal by no more than 1%. Therefore the experimental results obtained for alloys with an Al or Mg base [23-24] were not included in the approximated data fields.

For D−u equations of the form (1.1) or (1.2) the pressure may be expressed as an explicit function of the deformation $z = 1 - \rho_0/\rho = u/D$. For (1.1) this is the known expression $p = \rho_0 a_0^2 z(1 - a_1 z)^{-2}$, which admits of a transition to dimensionless variables [50-52]. For (1.2), if $a_1 z < 1$, and $\varepsilon \ll 1$, where

$$\varepsilon = \left[\frac{a_0 a_2 z^2}{(1 - a_1 z)^2 - 2a_0 a_2 z^2}\right]^2,$$

we have a simple equation [50]

$$p = \frac{\rho_0 a_0^2 z\,(1 + \varepsilon)}{(1 - a_1 z)^2 - 2a_0 a_2 z^2}. \tag{2.6}$$

It was found that for the values of coefficients obtained Eq. (2.6) is applicable in the ranges under study for all metals with adiabatic curves of types 2 and 3, where for $z < 0.4$ we may disregard the quantity ε in (2.6).

A total of 950 different shock-compression states for 32 elements were subjected to statistical analysis, after discarding the discrepant recordings which did not satisfy the Chauvenet criterion. Of this number, 175 points obtained in the Soviet Union (group "a") and 56 obtained on high-speed pneumatic systems fix the position of the adiabatic curves for their entire length. The remaining information is concentrated on the lower intervals of the ranges studied. On the average, ~30 shock-wave measurements were made for each metal. However, the investigators devoted different amounts of attention to different metals. Thus, the approximated data field for Be contained 68 shock-wave points, with 61 for Cu and 105 for Mg, but for Re and Cs the data fields contained only nine points each. In addition to the shock-wave measurements, the calculations for almost all the metals included four to six determinations of the initial velocity of sound, some of which were also discarded during the calculation process in accordance with the programmed criterion.

The parameters of the adiabatic curves and the confidence intervals obtained in the statistical processing are shown in Tables 4-7, where in every case, in addition to the element symbol, we give the range of pressures included in the approximation. The last column of each table shows the sources of information (a plus sign (+) indicates the data of Tables 1-3). Items 7-20 are the sources for group "a," 21-24 group "b," and 25-32 for group "c."

Table 4 includes 12 elements with a linear D−u relation (type 1). It shows the significance levels α for the linearity hypothesis, the number n_{sh} of statistically processed shock-wave points, and the relative errors

$$\nu = \left\{\sum_{i=1}^{n} \frac{g_i}{D_i^2}\,[D_i - D(u_i)]^2 \Big/ \sum_{i=1}^{n} g_i\right\}^{1/2} \tag{2.7}$$

which qualitatively characterize the averaged experimental dispersion of the original information. Here $D(u_i)$ is calculated by (1.1), n is the total number of points included in the calculation, and g_i is the coefficient of accuracy of the data used. Table 4 contains the parameters a_0, a_1 of the relations (1.1) with their confidence intervals Δa_0, Δa_1, the confidence deviations Δ_D^0, and the relative confidence errors (RCE) (Δ_D^0/D) for two characteristic points − the "center of gravity" of the experimental data $\langle u \rangle$ and u_{max}. Here and hereafter, the quantities a_0, $\langle u \rangle$, u_{max} are given in kilometers per second, Δa_0^0, Δ_D^0 in meters per second, pressures in gigapascals, and a_1, Δa_1^0 as dimensionless quantities.

The first eight metals of Table 4 have a_1 values close to the asymptotic value 1.25, and the D−u functions for these metals remain linear as their physical parameters vary greatly over wide ranges of u. For Mo, for

TABLE 4

Element p_{max}	α, %	n_y ν, %	a_0 a_1	$\Delta^0_{a_0}$ $\Delta^0_{a_1} \cdot 10^2$	$\langle u \rangle$ u_{max}	Δ^0_D	$\frac{\Delta^0_D}{D}$, %	Source
Li 71	71	27 1,33	4,760 1,065	48 0,8	3,0 9,2	32 80	0,40 0,55	[15, 30, 31]
K 87	39	22 0,75	1,991 1,17	16 0,4	1,7 8,5	11 45	0,28 0,38	[15, 30]
Be 92	23	68 0,83	7,993 1,132	29 0,9	1,8 4,0	15 35	0,15 0,28	[24, 28, 31]
Mg 176	53	105 1,15	4,540 1,238	22 0,6	2,0 7,4	12 54	0,17 0,30	[19, 24, 31, 32] [+]
Al 207	32	14 0,85	5,333 1,356	36 1,2	1,6 5,8	23 80	0,31 0,62	[+, 10, 20]
W 540	100	37 0,8	4,015 1,252	15 0,8	0,8 3,4	10 35	0,20 0,24	[12, 21, 29, 24]
Mo 1020	17	46 0,82	5,100 1,266	17 0,6	1,2 7,1	12 57	0,18 0,40	[+, 14, 24, 28, 29]
Re 625	77	9 1,06	4,068 1,347	31 2,2	0,6 3,4	24 97	0,48 1,12	[+, 24]
Ir 661	33	10 1,52	3,93 1,536	51 3,3	0,8 3,2	37 131	0,71 1,47	[+, 24]
Au 550	36	13 0,49	3,063 1,563	14 0,6	1,0 3,4	10 26	0,22 0,31	[+, 21, 28, 29]
Ba 217		4	1,108 1,369		6,0			[19]
Ga 326		4	2,501 1,560		5,1			[+]

example, the straight-line approximation according to the coefficients of Table 4 intersects (see Fig. 1) the interval of probable wave velocities recorded for $u = 10.7$ km/sec and $p \sim 2000$ GPa. It is probable that up to these pressures the linear form will be valid for W as well. For Ir and Au, with values of $a_1 > 1.50$, the linearity is associated with the predominant contribution of cold components of the pressures in the ranges studied so far. The behavior of Al and Be at pressures <200 GPa has not been determined unambiguously [13, 23, 32].

For barium and gallium there was no full-scale statistical processing because the experimental points available were too few. It was found that Ba undergoes a phase transition at 7 GPa [53] and Ga undergoes anomalous melting at the very beginning of the compression curve, at ~0.2 GPa [54]. The fact that their compressibilities do not have smooth curves is indicated by the sharp disagreement between the coefficients a_0 and the thermodynamic velocities of sound c_0. In the case of Ba the value of a_0 is 0.6 km/sec less than that of c_0, and in the case of Ga it is 0.7 km/sec less. For the other elements, the difference between a_0 and the most reliable values of c_0 is about 1%.

Table 5 describes the compressibility of 14 elements with parabolic D–u relations and negative (type 2) coefficients a_2, whose absolute values and confidence intervals are given in units of 10^2 sec/km.

All the metals in Table 5 have initial values of D'_u which considerably exceed $D'_{u\infty} \approx 1.25$. This fact explains the tendency of the adiabatic curves to decrease their slopes as u increases. The complex configuration of the curves for the confidence intervals Δ^0_D for the form (1.2) is fixed in Table 5 at four points – at $u = 0$ for the value of $\Delta^0_{a_0}$, at the minimum of the curve for $u = u_1$, at u_2 close to the second minimum or change of sign of the curvature, and at $u = u_{max}$. A large difference between a_0 and c_0 is found in the case of Cr and Sn, where it is due [53, 39] to phase transformation, and also in the case of Ce and Cs, which undergo a whole series of transitions under shock compression, as can be seen from the phase diagrams [54]. The elements Ba, Ga, Cr, Sn, Ce, and Cs exhaust the list of metals for which, according to the method we used, the values of c_0 were not included in the processing. The results relating to the other 26 metals considered in this section were obtained by including four to six values of c_0 in the approximated data field.

The data for Na, V, Nb, Ta, Co, and Rh with values of $a_2 > 0$ (type 3) are shown in Table 6, which is similar to Table 5. For five elements the values of a_1 are included between the limits of 1.11 and 1.23, while for Rh we find that $a_1 = 1.33$. Apart from Na, the other metals are transition elements with unfilled inner shells.

TABLE 5

Element p_{max}	n ν, % α, %	a_0 a_1 $-a_2 \cdot 10^2$	$\Delta^0_{a_0}$ $\Delta^0_{a_1} \cdot 10^2$ $\Delta^0_{a_2} \cdot 10^2$	u_1 u_2 u_{max}	Δ^0_D	$\frac{\Delta^0_D}{D}$, %	Source
Cr *	28	5,153	83	1,0	30	0,45	
	1,2	1,557	8,2	3,0	64	0,73	
400	1	4,23	1,2	4,8	170	1,46	[+, 24, 28, 29]
Ni *	26	4,501	69	1,0	44	0,72	
	1,39	1,627	5,2	4,6	84	0,73	[+, 11, 13, 23, 28,
995	0	2,64	0,5	7,4	200	1,32	29]
Cu *	61	3,899	24	0,8	14	0,27	
	0,93	1,520	2,2	3,2	30	0,34	[+, 10, 11, 13, 20]
976	2	0,71	0,3	7,4	93	0,63	[23, 24, 28, 29]
Ag *	17	3,178	50	0,6	36	0,86	
	1,20	1,733	5,9	2,2	53	0,78	
461	1	4,27	1,0	4,4	149	1,49	[+, 28, 29]
Zn *	25	3,031	30	1,0	20	0,43	
	0,93	1,608	2,4	3,6	38	0,44	[+, 11, 28, 29, 31]
826	0	2,24	0,28	8,0	168	1,16	
Cd*	24	2,434	37	0,8	28	0,73	
	1,4	1,759	3,2	2,8	43	0,61	[+, 11, 28, 29]
860	0	4,73	0,42	7,6	2,36	1,80	
Pd	29	3,955	28	0,6	16	0,32	
	0,66	1,701	4,9	1,4	19	0,31	
221	0	6,24	1,43	2,4	46	0,60	[24, 28, 29, 31]
Pt	61	3,605	34	0,6	20	0,46	
	1,17	1,560	4,6	1,6	28	0,42	
687	1	2,63	0,89	3,6	54	0,61	[22, 24, 28, 31]
In	15	2,430	34	0,5	27	0,84	[+, 28, 31]
	1,43	1,603	4,3	2,2	49	0,84	
350	3,5	2,07	0,80	4,9	168	1,72	
Tl	14	1,809	16	0,5	13	0,50	
	0,70	1,597	2,3	2	24	0,49	
435	1	2,47	0,4	4,4	68	0,81	[+, 28, 29]
Sn	19	2,437	51	1,8	21	0,39	
	0,65	1,688	2,9	4,4	38	0,92	[+, 11, 28, 29]
723	0	4,70	0,24	7,8	91	0,71	
Pb	20	1,981	22	0,7	16	0,52	
	0,93	1,603	2,2	3,2	35	0,53	[10, 11, 20, 28, 29]
967	1	3,78	0,20	7,3	106	0,91	
Cs	9	0,363	110	1,6	11	0,40	[30]
	0,36	1,583	7,8	3,2	22	0,44	
43	7	4,66	0,99	4,0	40	0,67	
Ce	33	0,934	42	1,4	14	0,48	
	1,05	1,944	2,9	4,0	35	0,46	[+, 19, 26, 27]
566	0	6,95	0,31	7,3	129	1,13	

As is shown by quantum-mechanics calculations [45], the decrease in compressibility is due in the case of V and Nb to the electron restructuring of their energy spectra and the anomalously large Gruneisen coefficients of the electrons. The same effects apparently occur in the case of Ta, Co, and Rh. The curvature of the D–u relation for Na is very slight. However, it is maintained even when the approximation interval is reduced to 4 km/sec, and, according to [43], it is due to the properties of the potential interaction of the Na atoms.

The adiabatic curves for V and Nb in [19] were assigned to type 4. The "smooth" description of them given here is based on the extensive information obtained in [24], statistically processed with due regard for the compressibility in the original state and at the highest pressures fixed in [19].

The nine elements indicated by asterisks in Tables 5 and 6 belong to types 2* and 3*, i.e., on the basis of statistical criteria, in the bounded but fairly broad intervals $0 < u < u_l$, they admit of a linear description. The equations of the adiabatic curves and their statistical characteristics for the linear segments are given in Table 7, which is similar to Table 4, and a comparison of these curves with the quadratic adiabatic curves for the same metals is given in Table 8. Here we indicate the abscissas (in km/sec) of the points m and n at which

TABLE 6

Element p_{max}	n v, % α, %	a_0 a_1 $a_2 \cdot 10^2$	$\Delta_{a_0}^0$ $\Delta_{a_1}^0 \cdot 10^2$ $\Delta_{a_2}^0 \cdot 10^2$	u_1 u_2 u_{max}	Δ_D^0	$\frac{\Delta_D^0}{D}$, %	Source
Na	24	2,624	27	1,2	16	0,34	
	0,73	1,188	1,8	4,0	27	0,36	[15, 30]
100	0	0,88	0,18	8,0	100	0,79	
V *	34	5,071	32	0,8	16	0,76	[19, 24, 29]
	0,82	1,185	3,2	2,2	29	0,37	
344	1	1,67	0,52	5,0	110	0,96	
Nb	36	4,472	32	0,8	16	0,30	
	0,83	1,114	3,8	2,0	26	0,38	
408	0	3,8	0,60	4,6	110	1,05	[+, 19, 24, 28, 31]
Ta*	26	3,431	29	0,7	19	0,40	
	1,05	1,159	3,0	1,5	26	0.50	
1097	0	2,48	0,40	5,9	142	1,27	[+, 14, 24, 28, 31]
Co	19	4,743	62	0,8	41	0,71	[+,28,29]
	1,18	1,227	6,3	2,0	48	0,65	
438	2	5,8	1,10	4,4	158	1,40	
Rh *	19	4,775	73	0,8	37	0,63	
	1,20	1,331	8,9	1,8	57	0,78	[+, 24, 28]
542	3	4,70	1,70	3,80	211	1,94	

TABLE 7

Element p_{max}	α, %	n v, %	a_0 a_1	$\Delta_{a_0}^0$ $\Delta_{a_1}^0 \cdot 10^2$	$\langle u \rangle$ u_l	Δ_D^0	$\frac{\Delta_D^0}{D}$, %	Source
Cr	10	27	5,205	46	1,0	22	0,33	
149		1,03	1,451	2,5	2,4	54	0,62	[24, 28, 29]
Ni	90	23	4,575	32	1,4	21	0,32	[+, 11, 23, 28, 29]
441		1,00	1,517	1,1	4,4	54	0,48	
Cu	14	51	3,915	14	1,2	9	0,16	[+, 10, 11, 23, 24,
413		0,81	1,495	0,6	4.4	32	0,31	28, 29]
Ag	100	14	3,170	29	1,0	19	0,40	
230		1,02	1.657	1,5	2,2	33	0,48	[+, 28, 29]
Zn	21	21	3,054	23	0,8	16	0,37	
202		1,08	1,541	1,1	3,4	45	0,54	[11, 28, 29, 31]
Cd	26	12	2,437	32	0,6	25	0,73	[11, 28, 29]
100		1,75	1,686	2,3	2,0	55	0,95	
V	41	34	5,068	23	1,0	13	0.21	
168		0,81	1,207	1,2	2.6	32	0,39	[24, 28]
Ta	74	22	3,429	14	0,8	9	0,23	
223		0,71	1,198	0,9	2,2	20	0,33	[14, 24, 31]
Rh	26	17	4.753	47	0,8	26	0,44	
218		1,18	1.416	2.9	2.2	6,3	0,80	[+, 24, 28]

the straight lines and the parabolas intersect (see Fig. 2) and the relative deviations (in percent) of the adiabatic curves from each other when $u = 0$ for $u_c = (u_m + u_n)/2$ and for the extreme point u_l of the linear approximation. For all of these elements except Ni, the difference is <1%, and, apart from a few exceptions, it does not exceed the RCE of Table 7.

Thus, depending on the pressure level under consideration and the purposes aimed at, for nine metals which have adiabatic curves of types 2* and type 3* we can use either "solid" parabolic representations (Tables 5, 6) or bounded-linear representations (Table 7). This conclusion is somewhat inapplicable only in the case of Ni, for which the a_0 of the quadratic form differs by 1.7% in the downward direction both from the "linear" a_0 and from the most-probable thermodynamic velocity of sound $c_0 = 4.58$ km/sec at normal conditions. For a precision approximation including all of the data it is desirable in this case to use a piecewise smooth approximation given by the formulas of Tables 5 and 7, with a point of conjugacy at $u = 3.32$ km/sec.

TABLE 8

Element	u_m	u_n	$\left(\frac{\Delta}{D}\right)_0$, %	$\left(\frac{\Delta}{D}\right)_c$, %	$\left(\frac{\Delta}{D}\right)_l$, %
Cr	0,67	1,84	—0,95	0,20	—0,59
Ni	0,84	3,32	—1,64	0,50	—0,93
Cu	0,84	2.68	—0,41	0,09	—0,43
Ag	0,10	1,88	—0,25	0,85	—0,48
Zn	0,40	2,59	—0,76	0,52	—0,65
Cd	0,04	0.87	—0,12	0,61	—0,77
V	0,15	1,16	0,06	—0,13	0,73
Ta	0,05	1,52	0,06	—0,30	0,60
Rh	0,31	1,50	0,47	—0,25	0,51

In most of the earlier publications for the other 11 elements of Table 5 and Table 6 which belong to types 2 and 3, over intervals of different lengths, the D(u) equations were given in the form of linear binomials (1.1). Let us find the admissible boundaries of such an approximation, which is convenient for many applications. It is easy to show that for each selected interval of linearity (0, u_L) it is possible to find a secant whose distance from the parabola for $u=0$, $u_L/2$, and u_L will be $\Delta = |a_2| u_L^2/8$, all three distances having the same absolute value. The coefficients of the secant will be

$$a_{0L} = a_0 - a_2 u_L^2/8, \quad a_{1L} = a_1 + a_2 u_L.$$

For very small differences ($\Delta = 10^{-2} a_0$) the intervals of the approximate linear description will be the following: ~1 km/sec for Cs and Ce, ~2 km/sec for Pd, Sn, Pb, Co, and Tl, slightly more than 3 km/sec for Nb, In, and Pt, and 5.5 km/sec for Na.

The characteristics so calculated for the initial segments of the adiabatic curves of these metals, like the linear approximations of Tables 1 and 4, are close in the nominal values of their coefficients to the expressions given for the same elements [28, 15, 19, 7, 24]. For 20 metals the extended ranges of the parameters are described in this study without loss of accuracy by the quadratic trinomials of Tables 5 and 6.

The most important statistical characteristic obtained consists in the confidence intervals determining the errors in the positions of the shock adiabatic curves of the metals. For the indicated values of u the values of Δ_D^0 are given in Tables 4–7. Figure 6a shows the variations of the functions $\Delta_D^0(u)$ for Mo (type 1), Pb (type 2), and Co (type 3). Analogous curves are shown in Fig. 6b for Cu, Ni (type 2*), and V (type 3*). For Cu and Ni the figure shows the variation for the complete parabolic description (solid curve), and for Cu it also shows the variation for the bounded-linear description (dashed curve). As shown by the graphs and tables, a feature common to all the curves is a deep minimum at ~1 km/sec. The largest values of Δ_D^0 are attained at the right end of the intervals under consideration, and a slightly smaller value is attained at the left end (when $u=0$). The values of Δ_D^0 depend on the number and statistical weight of the points, on their experimental dispersion, and also on the analytic form used in the approximation. For a linear law of increase of D the values of Δ_D^0 are smaller than for a quadratic law; in the latter case, more regression coefficients in the D–u relations must be determined.

Using the examples of V, Pb, Cu, Cr, Mo, Li, and Be, we verified the effect produced on Δ_D^0 and on the equations obtained for the adiabatic curves by the choice of the statistical weight W_i in the form $W_i = g_i D_i^{-2}$ or $W_i = g_i$, i.e., when the form M was minimized on the basis of relative or absolute deviations. In particular, for V and Pb in the second case we obtained the formulas

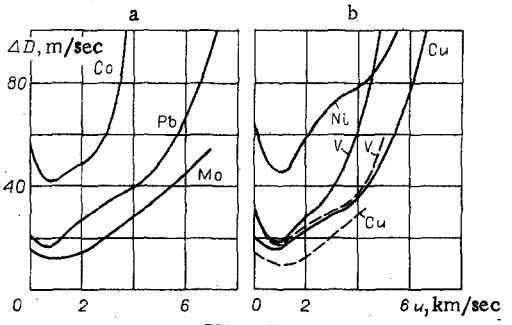

Fig. 6

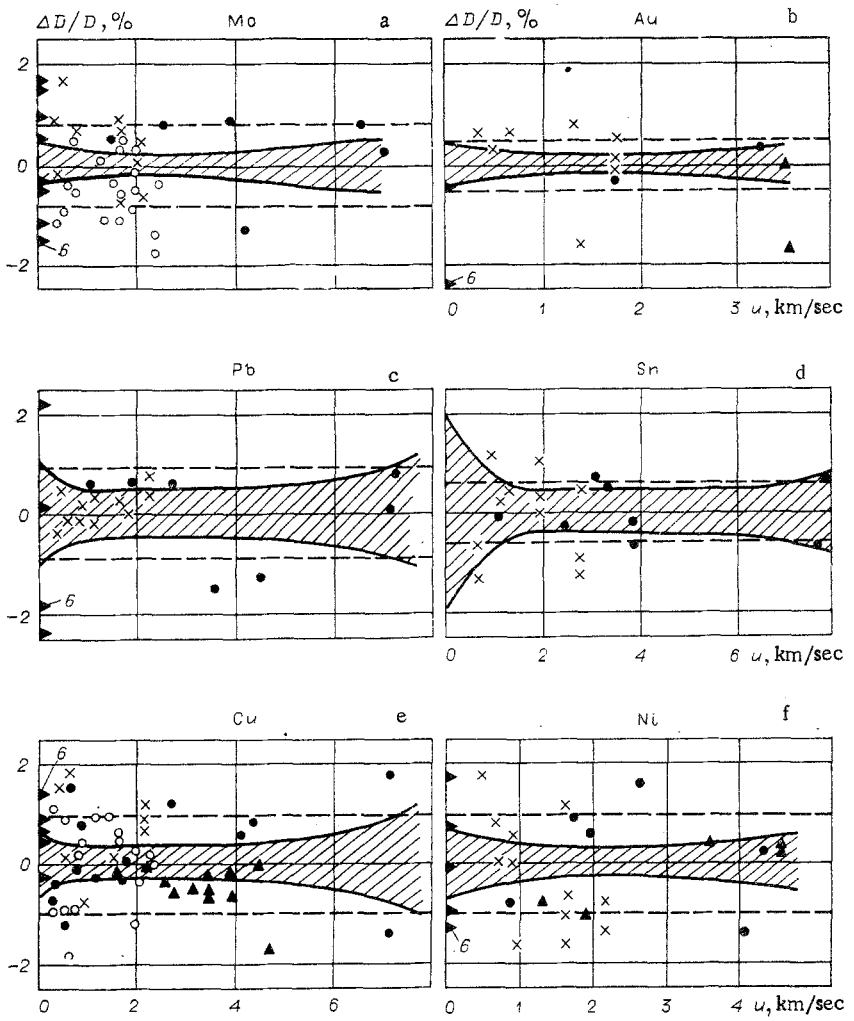

Fig. 7

$$\begin{aligned} \text{V}: D &= 5.072 + 1.174u + 1{,}99\cdot 10^{-2}u^2, \\ \text{Pb}: D &= 2.004 + 1.571u - 3.3\cdot 10^{-2}u^2, \end{aligned} \tag{2.8}$$

which are practically identical with the relations given above: The wave velocities calculated by (2.8) and calculated by the coefficients of Tables 5 and 6 differ by a fraction of 1%. On the other hand, when we pass from $W_i = g_i D_i^{-2}$ to $W_i = g_i$, the values of Δ_D^0 for large values of u decrease. The two variants of the choice of weight for V are associated with the solid and dashed curves, respectively, in Fig. 6b. The unrealistically small values of the confidence intervals for large values of u obtained for $W_i = g_i$ confirmed the advisability of making the approximations used in this study on the basis of the relative deviations of the experimental data.

In the solution of many problems it is essential to know the values of the relative confidence deviations (RCE). For some metals the $(\Delta_D^0/D) - u$ diagrams in Fig. 7 are given against the background of the relative deviations of the experimental data we processed. The values of c_0 are indicated on the ordinate axis by the points 6, while the rest of the notation is the same as in Figs. 1-3. Unlike the case of Δ_D^0, the RCE contours are drawn as bands in the middle zone of approximately constant width, which extend only to the edges of the intervals studied. The dashed lines in the diagrams of Fig. 7 indicate the values of $\pm \nu$ calculated from (2.7) and characterizing the so-called "apparent" error of the experiment [47]. Over almost the entire extent of the boundary the RCE are within the band $\pm \nu$. The difference between the RCE and ν is especially large in the case of Mo and other linearly approximated metals. The diagrams in Fig. 7 also illustrate the characteristic distribution of the dynamic information over the amplitude ranges which are given on the lower scales by the values of the mass velocities. The points obtained with explosive systems outside the Soviet Union and belonging to groups "b" and "c" are predominant in the intervals of the first 2-2.5 km/sec and pressures of 1.5-2 Mbar. (These limits refer to the elements of Fig. 7 which have medium and large atomic numbers. For light metals they are naturally displaced in the direction of larger values of u and smaller values of p.) Here we find the "centers of gravity" of the experimental measurements and the narrowest segments of Δ_D^0 and RCE.

TABLE 9

p, GPa	Element	$\left(\frac{\Delta_p^0}{p}\right)_z$, %	$\left(\frac{\Delta_z^0}{z}\right)_p$, %	$(\Delta_\delta^0)_p \cdot 10^2$	Element	$\left(\frac{\Delta_p^0}{p}\right)_z$, %	$\left(\frac{\Delta_z^0}{z}\right)_p$, %	$(\Delta_\delta^0)_p \cdot 10^2$
50	Pb	1,87	0,67	0,44	Cu	0,74	0,44	0,12
100		2,45	0,68	0,70		0,92	0,45	0,23
200		2,96	0,66	1,04		1,09	0,48	0,38
400	(Table 5)	2,7	0,61	1,16	(Table 5)	1,23	0,55	0,69
800		4,41	0,88	2,21		1,98	1,11	2,03
1000		5,3	1,22	5,73		2,36	1,46	2,92
50		0,33	0,23	0,04	Ni	0,96	0,58	0,14
100	Mo	0,48	0,28	0,09		0,92	0,45	0,18
200		0,63	0,29	0,17		1,27	0,46	0,29
400	(Table 4)	1,10	0,38	0,40	(Table 7)	2,34	0,58	0,64
800		1,88	0,47	0,81				
1000		2,20	0,49	0,94				

Pressures of order 2-5 Mbar have been studied chiefly on explosive systems of group "a" (except for Be and Pt), and also on pneumatic apparatus (Mg, Cu, Ni, Pt, W, Au, and Be). As is shown by a comparison on the diagrams of Fig. 7 (Au, Cu, Ni), there are no systematic differences between the data of these two methods, which are denoted here, as before, by the points 2 and 5. The characteristics of the compressibility up to 8-9 Mbar for the metals statistically analyzed here (Ni, Cu, Pb, Sn, Zn, Cd, Mo, Ce) were obtained only in the investigations of the first group, which determined the configurations of the adiabatic curves in this region and their positions in the D–u plane with maximum values of RCE ~1%.

The analysis we carried out enables us to estimate the true accuracy associated with the shock adiabatic curves when we pass from the function D(u) to other variables. Applying the theory of error transfer to this, we have

$$\left(\frac{\Delta_u^0}{u}\right)_D = \frac{1}{zD_u'}\left(\frac{\Delta_D^0}{D}\right)_u. \tag{2.9}$$

Making use, in addition, of the relations at the discontinuity we can pass to thermodynamic parameters, which gives us

$$\left(\frac{\Delta_p^0}{p}\right)_z \approx \frac{2}{1-zD_u'}\left(\frac{\Delta_D^0}{D}\right)_u; \tag{2.10}$$

$$\left(\frac{\Delta_z^0}{z}\right)_p \approx \frac{2}{1+zD_u'}\left(\frac{\Delta_D^0}{D}\right)_u. \tag{2.11}$$

Here the subscript after the parentheses in (2.2)-(2.4) indicates that the corresponding quantity is constant when we calculate the random deviation of the function. Thus, on the verticals and horizontals of the insets in Fig. 4 the contours of the shaded strips cut off the quantities $\pm (\Delta_p^0/p)_z$, $\pm (\Delta_z^0/z)_p$, indicated in percent.

The degree of determinacy of our ideas concerning the dynamic compressibility of metals is more completely illustrated by using the examples of Pb, Mo, Cu, and Ni given in Table 9, calculated on the basis of (2.10) and (2.11); the table also indicates the errors for the degree of compression $\delta = \rho/\rho_0$, which are calculated by the formula $\Delta_\delta^0 = \delta(\delta-1)\Delta z/z$. For various metals, the dynamic pressures at a given volumetric deformation at the level of 10 Mbar are now known with an accuracy of ± 2 to ± 6%. At 4 Mbar the confidence error decreases to 1-3%, and at 1 Mbar to 0.5-2%.

The errors $\Delta_{a_i}^0$ found in this study characterize the probable deviations of the coefficients of the D(u) equations from their true values. On the average, the deviations of the $\Delta_{a_0}^0/a_0$ amount to 0.3% for adiabatic curves of types 1, 2*, and 3* (Tables 4 and 7) and to 0.5% for the quadratic approximations. We have determined with this accuracy the coefficients a_0 representing the most reliable values of the velocity of sound c_0 at normal conditions. Actually, in finding these, in addition to the experimental values of c_0 found by other methods, from which the discrepant values were discarded in the calculation process, we included with a large effective weight the shock-wave measurements which determined in the D–u plane the position of the initial segment of the adiabatic curve. For isentropic bulk compression moduli, $K_{S_0} = \rho_0 c_0^2$ the possible errors are equal to 0.6-1.0%. The coefficients a_1 in Eqs. (1.1) and (1.2) are associated with the derivatives of the bulk compression modulus for p = 0 by the known relation [53]: $4a_1 = (\partial K_S/\partial p)_{S_0} + 1$. From this, if we are discussing equations of the Murnaghan type, $p = \frac{\rho_0 c_0^2}{B}[(\rho/\rho_0)^k - 1]$, $4a_1 = B + 1$ and $\Delta_k^0 = 4\Delta_{a_1}^0$. For the metals in Tables 4 and

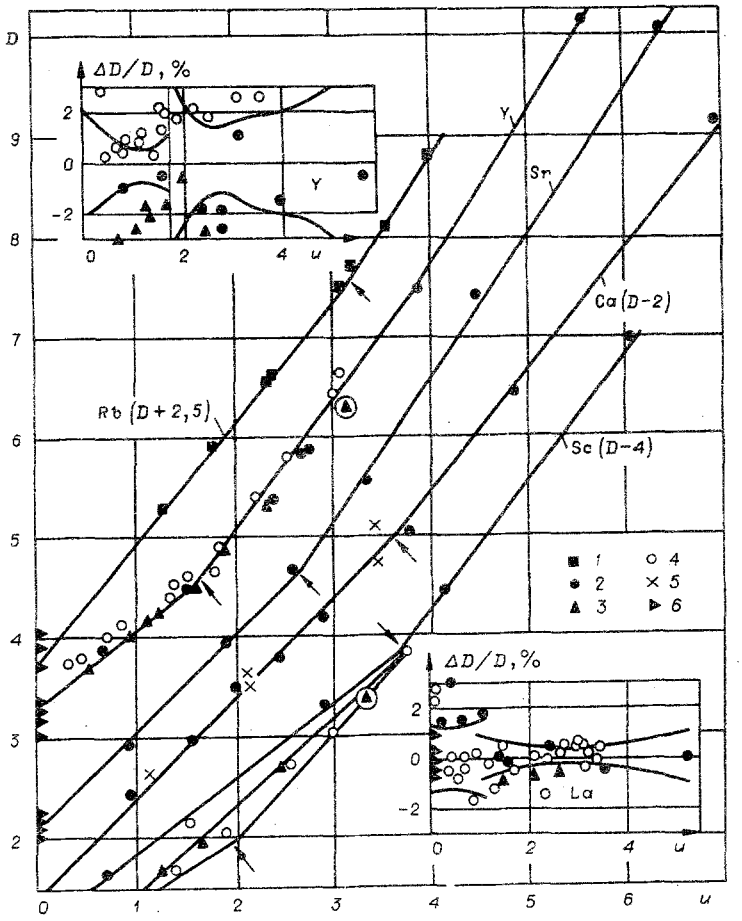

Fig. 8

7 we have an average value of $\Delta_l^0 = 0.05$, and for quadratic approximations of other metals we have 0.14. These accuracies are considerably better than those attainable by ultrasonic determinations of the Murnaghan coefficients. The third parameter in Eq. (1.2) (the coefficient a_2) was found with an average relative error of 10%.

Let us estimate the possibilities opened by the use of the experimentally studied metals as dynamic tensometers. The dynamic pressures for an adiabatic curve which is known to some specific degree of accuracy can be determined by making measurements on specimens to determine one parameter alone – the mass velocity or the wave velocity. The resulting error is due to two sources: the indeterminacy of present-day ideas concerning the position of the shock adiabatic curves, i.e., the values of the RCE, and the inaccuracy of the experimental measurements, i.e., the quantities $(\Delta^E u/u)$ or $(\Delta^E D/D)$. Considering the errors independent and using (2.9) and the relations at the discontinuity, we obtain the following estimates for the accuracy of the recording of the pressures for the measurements of u and D, respectively:

$$\frac{\Delta_p^0}{p} = \left[\left(\frac{\Delta^E u}{u}\right)^2 (1 + zD_u')^2 + \left(\frac{\Delta_D^0}{D}\right)^2\right]^{1/2}; \tag{2.12}$$

$$\frac{\Delta_p^0}{p} = \frac{1}{zD_u'}\left[(1 + zD_u')^2 \left(\frac{\Delta^E D}{D}\right)^2 + \left(\frac{\Delta_D^0}{D}\right)^2\right]^{1/2}. \tag{2.13}$$

As can be seen from the structure of the formulas and the approximate equation $(\Delta^E u/u) \approx (\Delta^E D/D)$, because (2.13) contains the factor $(zD_u')^{-1}$, it is preferable, especially for small values of z ($p < 50$ GPa), to determine the pressures from the value of the mass velocity.

For idealized "absolutely accurate" recordings the error $(\Delta_p^0/p) \approx (\Delta_D^0/D)$ varies from several tenths of 1 to 1%. In practice, when we use the highly accurate D–u relations obtained above, the main contribution to the error in finding p comes from the experimental inaccuracy of a specific single measurement of $(\Delta^E u/u)$ or $(\Delta^E D/D)$, which, as a rule, is greater than the value of the RCE.

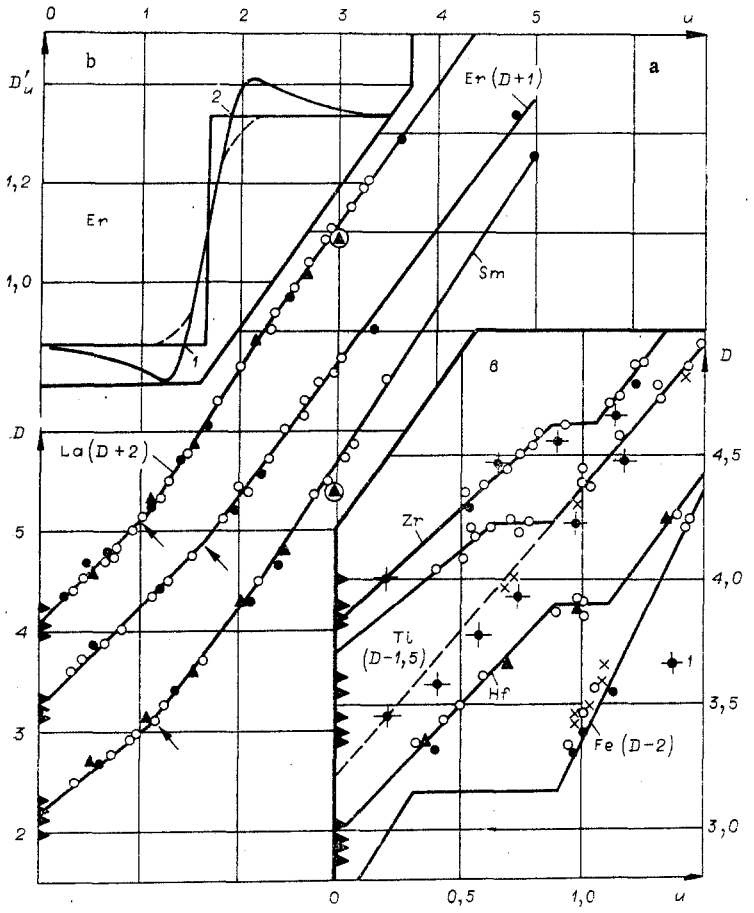

Fig. 9

3. Nonsmooth Adiabatic Curves for 22 Elements. General Laws

Nonsmooth Hugoniot adiabatic curves (Figs. 8, 9a), which are assigned to type 4, are characteristic of 17 elements found on the left side of the periodic table [7]. These were observed in the case of Rb [30], Ca, and Sr [17, 19], and, according to [19, 26, 27], also in the case of Sc, Y, and all the rare-earth elements (REE) of period VI that were studied. Such adiabatic curves contain critical points or narrow regions separating the shallower lower parts of the curves, hereafter indicated by the subscript "l" from the steeper upper portions (subscript "u"). Traditionally, both segments are described by linear relations in the kinematic variables: the wave velocity D and the mass velocity u. In what follows, we shall use the more general form

$$D_u = a_{0u} + a_{1u}u, \; D_l = a_{0l} + a_{1l}u + a_{2l}u^2, \tag{3.1}$$

where the coefficient a_{2l} may be negative, positive, or zero.

The presence of break-points in the compression curves is due [45, 7] to the shift of the outer electrons to the inner orbitals and the formation of compact electron configurations with low compressibility.

According to the estimates of [27], the singularities of the adiabatic curves lie near the melting curves. Since [55] discontinuous variation of elasticity is not characteristic of the liquid state of a metal, it follows that for a more complete understanding of the physical nature of the processes taking place it is of the first importance to clarify the possible width of the transition zone and the accuracy of its localization on the scale of pressure and temperatures. As in the case of other metals, the following analysis has the additional purpose of finding the most reliable D(u) functions and confidence intervals for the coefficients appearing in them and for the wave velocities. These same problems are also solved for stepwise D(u) curves (Fig. 9c) of type 5, which are formed in phase transitions of the first kind.

Let us now consider the adiabatic curves of type 4 shown in Figs. 8 and 9a, where the sonic data are the points 6 and the shock-wave data are the points 1-5; in the case of Rb (the points 1) most of the points lie on the lower branch, while the two upper ones lie on a ray passing through the origin. According to [30], the adiabatic curve of Rb is described by the equations $D_u = 1.232 + 1.184u$, $D_l = 1.567u$ (here and hereafter, the velocities D and u are given in km/sec). In the case of Sr, a well-defined break-point angle is formed [19] by

the straight lines $D_u = 2.10 + 0.94u$, $D_l = 0.58 + 1.5u$. The two metals were not analyzed statistically, since there were not enough recordings for the upper branches. In the case of Sc it is desirable to process all the information together, owing to the large deviations between the data of [19, 26, 27], indicated in Figs. 8 and 9a by the points 2-4, respectively. Here we can judge with a certain degree of determinacy only the slopes $a_{1u} = 0.64$-0.74, $a_{1l} = 1.0$-1.3. The systematic differences between the measurements obtained by different investigators were also found in the case of Y. As can be seen from the "divergence diagram" shown in the upper inset of Fig. 8, the experimental points of [19, 26] in the case of Y lie below the approximating curve, whereas in [27] they lie above it. The same distribution of data, but with a smaller amplitude of dispersion, is observed in the case of Dy. For a wide group of other REE we find satisfactory agreement between the results obtained by different authors. Typical of these is the case of La, shown in the lower inset of Fig. 8. The actual D–u diagram for La and the characteristic functions for two other rare-earth metals (Er and Sm) are shown in Fig. 9a.

Since the reasons for the systematic discrepancies are unknown, the shock-wave data of various authors for REE were taken into account with the same significance coefficient $g = 1$. The same weight was used in processing the values of the isentropic volumetric velocities of sound obtained by different methods: from the velocities of longitudinal and transverse waves in polycrystals [26, 27], those calculated from the velocities of ultrasonic waves along different directions in a single crystal [41], those found from analytic formulas describing the behavior of the curves of isothermal compression [35, 36-39], and those found from the values of the elastic moduli of polycrystalline specimens at normal conditions [35].

To clarify the possible transition-zone dimensions consistent with the experiments, we shall describe both branches of the curve of dynamic compression of type 4 by a continuous analytic function which differs substantially from a function of the form (3.1) only in a region of width $2l$. Such properties in the case of $a_{2l} = 0$ are found, in particular, in the function

$$D_L(u) = D_{crit} + (1/2)(u - u_{crit})[a_{1l} + a_{1u} + (a_{1l} - a_{1u})\tanh[(u - u_{crit})/l]] \tag{3.2}$$

which, for values of l that tend to zero, passes into the asymptote equation, equivalent to (3.2):

$$D_A(u) = D_{crit} + (1/2)(u - u_{crit})[a_{1l} + a_{1u} + (a_{1l} - a_{1u})\operatorname{sign}(u - u_{crit})]. \tag{3.3}$$

For any finite l, the curve (3.2) is tangent at the point u_{crit}, D_{crit} of intersection of the straight lines, deviating downward, for $u_1 = u_{crit} - 0.63l$ and $u_2 = u_{crit} + 0.63l$, by a maximum amount

$$\delta D = D_L - D_A = -0.14(a_{1l} - a_{1crit})l. \tag{3.4}$$

The nature of the variation of the derivative $D'_L(u)$ in the case of Er for $2l = 600$ m/sec is shown in Fig. 9b. Here the distance of $1.26l = 380$ m/sec between points 1 and 2 is the effective smoothing interval, in which the derivative increases almost linearly from the value $a_{1u} = 0.87$ to $a_{1l} = 1.33$. The formation of the extended transition zone of 25 GPa is attained as a result of slight variations in the wave velocities which do not exceed 20 m/sec, according to (3.4). A very similar result is obtained for a monotonic increase (the dashed curve) of the derivative within the same interval of 380 m/sec, when the maximum deviation from the linear-discontinuous description at $u = u_{crit}$ is equal to 27 m/sec. Thus, for any structure of the transition zone the attainable accuracy of the shock-wave measurements is not enough to distinguish between two different physical situations: the discontinuous onset of states with low compressibility at critical transition parameters and the gradual increase in the elasticity of the metal over a broad range of pressures up to and beyond 20 GPa. This negative result leads us at the same time to the important conclusion that it is permissible and, from a practical standpoint, advisable to introduce for approximation purposes a set of effective break-points and a segmented description of the dynamic-compression curves by means of Eqs. (3.1). The question of the physical reality of the break-points still remains undecided. It may be answered by means of experimental recordings of the derivatives of the compression curves on the basis of the values of the velocities of sound behind the shock-wave front for waves with different amplitudes, for example by the lateral-unloading method of [56].

Statisical processing of the results, making use of many regression parameters of Eq. (3.2), is a difficult problem. An approximate method consists in first subdividing the entire experimental data field of N points into a "lower" and an "upper" set and carrying out an independent statistical analysis for each of them on the basis of the algorithms available for equations of the type (3.1).

By definition, the optimal distribution of the data between the lower and upper segments of the adiabatic curves leads to the most accurate approximation, when the parameter

$$\bar{v} = \left[\sum_{i=1}^{n_u}(D_u - D_i)^2 W_i + \sum_{i=n_u+1}^{N}(D_l - D_i)^2 W_i\right]^{1/2} \Big/ N^{1/2}, \tag{3.5}$$

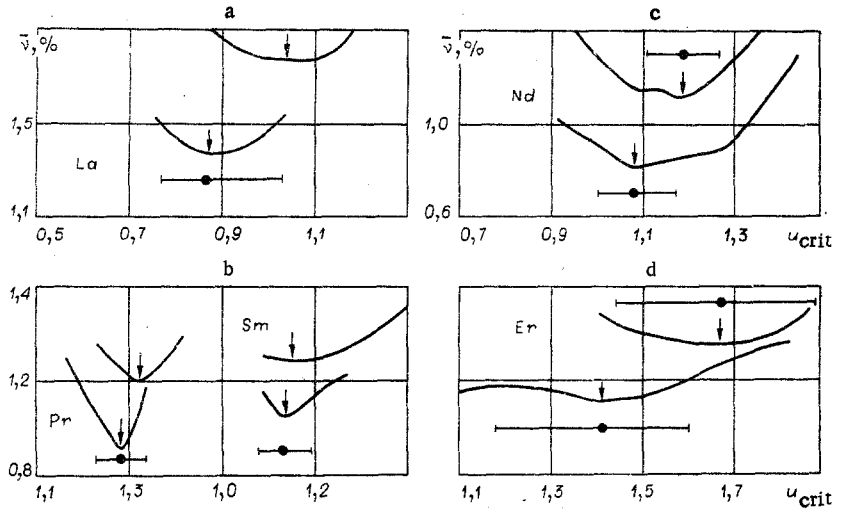

Fig. 10

averaging the deviations for the lower set n_u and the upper set n_l ($n_u + n_l = N$), takes on its minimum value.

A new method was devised for a quantitative determination of the possible errors in the value of u_{crit} but only for linear variants of (3.1). In this case the intersection of the two partial descriptions m, l of the optimal subdivision is obtained for

$$u_{crit}^{m,l} = \frac{a_{0u}^{m} - a_{0l}^{l}}{a_{1l}^{l} - a_{1u}^{m}}. \tag{3.6}$$

The set $u_{crit}^{m,l}$ forms a new set derived from the probability characteristics of the coefficients on the right side of (3.6). Calculation of the number m, l of the variants distinguishes on the mass-velocity axis around the nominal point u_{crit} the confidence intervals $2\Delta_{u_{crit}}^{0} = u_2 - u_1$ in which the break point will be found with probability z, in particular q = 0.68. From the structure of Eq. (3.6) it follows that the quantity $u_2 - u_1$ is inversely proportional to the difference $a_{1l} - a_{1u}$ between the nominal slopes of the D(u) graphs.

Examples of the calculation of the $\bar{\nu}(u_{crit})$ on the basis of (3.5) for different methods of subdivision of the data between the "phases" with high and low pressure are shown in Fig. 10 for five different REE. The upper curves were obtained by processing all the dynamic data and the values of the velocity of sound for p = 0. The lower curves, which have a smaller experimental dispersion, were obtained only from the shock-wave measurements of [27]. In the calculations we took $W_i = D_i^{-2}$. The horizontal segments on the graphs indicate the confidence intervals $\Delta_{u_{crit}}^{0}$ for the break points calculated according to the algorithms. The degree of localization now achieved varies from metal to metal. For Pr and Sm the indeterminacy of the position is ~100 m/sec. For La and Nd it is ~200 m/sec, and for Er it is ~500 m/sec. There is a clearly visible displacement of the break points in the direction of larger values of u_{crit} which was obtained by processing all the items of information together. Therefore, in order to obtain the nominal parameters of the break points and analyze their correlation with the melting of the metal, it is preferable to confine ourselves to processing the measurements of [27]. They are fairly numerous, were obtained by a uniform method, and do not include points relating to especially high pressures. The results of the processing for REE are given in Table 10. Here we give for the two branches the levels of significance α of the linear hypothesis, the nominal coefficients of Eqs. (3.1) for linear variants, the critical values of the pressure p_{crit} (together with the symbol of the element), the wave velocities D_{crit}, and the mass velocity u_{crit}, and in the last column we indicate the limits of u_{crit} for the segment within which the break-points of the adiabatic curves will be included with probability q = 0.68.* The statistical analysis was carried out for the minimization of the functionals M with respect to the relative deviations, i.e., with $W_i = D_i^{-2}$. The nominal coefficients of the approximations are close to the previous ones found in [27]. In the same way, for all elements except La, in the new processing method the points of conjugacy of the branches differ in mass velocity by no more than 60 m/sec from the data of [27].

The estimates of the accuracy of the localization of the break-points contain essentially new information. The shaded areas in Fig. 11 represent the data of the last column of Table 10, converted to pressures, for the

*The velocities and the coefficients a_0 in the tables are given in kilometers per second, and the pressures in gigapascals.

TABLE 10

Element p_{crit}	α, %	a_{0u} a_{0l}	a_{1u} a_{1l}	D_{crit}	u_{crit}	Limits u_{crit}
Y 35,90	6 34	3,424 2,391	0,733 1,346	4,65	1,68	1,50—1,85
La 15,67	76 47	2,082 1,586	0,938 1,504	2,90	0,88	0,78—1,03
Pr 27,10	17 35	2,101 0,936	0,781 1,685	3,10	1,29	1,24—1,34
Nd 23,00	12 9	2,188 1,531	0,794 1,401	3,05	1,08	0,99—1,17
Sm 26,20	67 28	2,55 1,580	0,746 1,341	3,10	1,14	1,08—1,19
Gd 30,00	53 62	2,195 1,793	0,927 1,272	3,27	1,16	0,96—1,33
Tb 35,10	62 62	2,176 1,748	0,949 1,287	3,38	1,27	1,10—1,42
Dy 30,40	88 64	2,28 1,907	0,887 1,223	3,26	1,11	1,01—1,22
Ho 42,80	48 50	2,272 1,925	0,959 1,213	3,58	1,37	0,88—1,63
Er 45,50	11 49	2,345 1,692	0,870 1,334	3,57	1,41	1,18—1,63
Tu 40,70	36 97	2,259 1,889	0,907 1,197	3,42	1,28	0,94—1,63
Yb 15,65	90 83	1,451 0,875	0,836 1,422	2,16	0,98	0,93—1,04

confidence intervals of the critical states. The horizontal segments in the diagram indicate the levels of shock-wave pressures at which, according to the estimates given by the authors of [27], we will have melting of the metal, and in the case of Gd we will have a polymorphic transition. As can be seen from the diagram, in the case of most of the metals, the assumed pressures of the phase transformations lie outside the confidence intervals or on their boundary, 3-6 GPa away from the nominal values of p_{crit}. For some of the metals (La, Nd, Gd, Tb) the close agreement obtained in [27] is based on erroneous values of the break-point pressures. (The data given in the table and in the graphs of the present study disagree with the values calculated from the coefficients of the D(u) functions given in [27].) In the case of Dy, Er, Ho, and Tu the melting parameters lie inside the intervals, close to the nominal values of p_{crit}. However, this agreement gives us little physical information, since the absolute dimensions of the confidence intervals for Dy, Er, Ho, and Tu are extremely large (from 8 to 30 GPa).

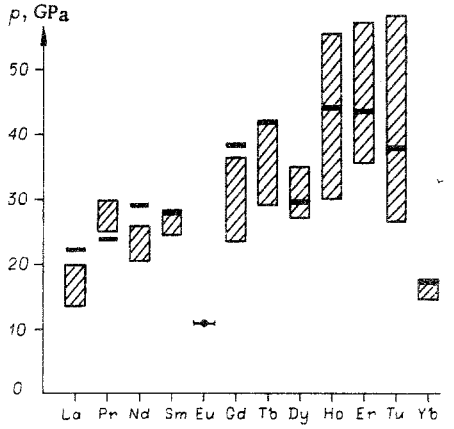

Fig. 11

TABLE 11

Element ρ_{crit}	α, %	a_{0u} a_{0l}	a_{1u} a_{1l}	$a_{2l}\cdot 10^2$	D	u_{crit}	Δ_D^0, m/sec	$\langle u \rangle$ u_{max}	Δ_D^0, m/sec
La 20,1	75 0	2,064 1,391	1.012 1.702	— —4,56	3,12	1.05	50 27	1,8 5,3	14 114
Pr 28	89 4	2,109 0,759	0,779 1,858	— —4.3	3.14	1,32	15 53	2,0 5.2	29 263
Nd 26,2	2 11	2,171 1,424	0,823 1,450	—	3,15	1,19	23 24	2,1 5.1	17 69
Sm 27,2	43 0	2,224 1,838	0,806 1,062	6.68	3,15	1.16	41 29	1.7 5,0	19 147
Gd 29,9	20 94	2,197 1,801	0,931 1,274	— —	3.27	1,16	22 28	2,1 7,1	18 107
Er 58,5	60 75	2,287 1,579	0,947 1,370	— —	3.87	1.67	41 48	2.5 4,8	27 117
Yb 15,4	94 94	1,435 0,866	0,865 1,419	— —	2,12	1,03	23 22	1,6 5,2	15 93
Y 34,6	14 18	3.381 2,795	0,725 0,982	— 6,00	4.58	1,65	52 178	2,4 5,6	77 436
Dy 45,10	83 22	2,252 1,844	0,926 1,157	— 3,09	3,62	1,48	32 61	2,0 4,9	41 247
Ho 36,6	87 19	2,291 2,150	0,934 0,986	— 5,26	3,44	1,22	12 48	1,6 4,8	28 240
Lu 74,7	— —	2,20 0,98	1,00 1,65	— —	4,08	1,88	— —	— —	— —
Ca 39,3	15 76	3,438 2,405	0,968 1,248	— —	7,01	3,69	85 270	4,6 7,00	196 445

At the same time, the data on Eu, which has an adiabatic curve of type 5, and the general form of the diagram indicate that there is a certain correlation existing between melting and the electron transitions. We do not know at present whether there is a physical connection between these processes or whether both of them are the result of lanthanide compression [57]. The solution of this problem requires the use of methods which will make it possible to record experimentally the melting and the elasticity of the metal behind the shock-wave front on the basis of the velocity of propagation of small disturbances [56].

Simultaneous processing of the data [19, 26, 18, 27] and Table 3 enables us to follow the behavior of the adiabatic curves of type 4 to pressures above 300 GPa (600 GPa in the case of Gd) and find, as for other metals, the accuracy of their determination. The results obtained are shown in Table 11.* The first seven columns of Table 11 contain the same information as Table 10. On the right-hand side of Table 11, instead of the limits for u_{crit}, we give the statistical characteristics of the adiabatic curves: the values of Δ_D^0 for the lower and upper branches in the case of u_{crit} and for the upper branch in the case of $\langle u \rangle$ and u_{max}, where Δ_D^0 will be minimal and maximal. For La, Pr, Nd, Sm, Gd, Er, and Yb the simultaneous processing satisfactorily reproduces the approximations of Table 10, although in the case of La, Nd, and Er it leads to substantial displacements of the break-points. Because of the large experimental dispersion and the systematic deviations of the measurements, we obtained poorer agreement of the approximations and larger confidence intervals in the case of Y, Dy, and Ho. For Lu, since the recordings in [19] were few in number, Table 11 gives only the nominal values of the coefficients. For Ca, since there is little difference in the slopes a_{1u} and a_{1l} (see Fig. 8), analysis of the data of [19, 31] (the points 2 and 5) yielded a large indeterminacy in the location of the break-point. The adiabatic curve for Ca could be described with equal justification by a single parabolic D(u) curve. The existence of electron transitions and states of the metal which have different compressibilities is, however, confirmed for the case of Ca by quantum-mechanical calculations and measurements of electrical resistance [58].

Among the metallic elements which undergo phase transitions of the first kind, high-pressure and low-pressure phases in dynamic experiments were recorded for Ti, Zr, Hf, Eu, and Fe. In the classification we

*The acoustic data were taken into account for all the elements of the table except Y, Dy, and Ho.

TABLE 12

Element p_{crit}	α, %	a_{0u} a_{0l}	a_{1u} a_{1l}	D_K	$u_{crit.upp.}$ $u_{crit.low.}$	Δ^0_D, m/sec	$\langle u \rangle$ u_{max}	Δ^0_D, m/sec	Source
Ti 16,7	— 86	5,22 4,722	0,767 1,130	5.72	0,65 0,88	— 29	2,0 9,4	20 130	[28, 29, 14] [24, 23, +]
Zr 26,5	5 25	3,83 3,236	0,914 1,301	4,63	0,88 1,07	18 16	1.8 5,2	13 50	[28, 31] [19, 24]
Hf 44,5	5 64	2,948 2,422	1,069 1,325	3,89	0.88 1,11	52 41	2,0 4,4	23 99	[18, 24] [26]
Eu 10,6	77 27	1,720 1,023	0,848 1,303	2,43	0,84 1,08	48 50	2,1 4,0	34 89	[18, 26] [27]

have adopted, the adiabatic curves of these metals belong to type 5, i.e., consist of three segments (Fig. 9c): the adiabatic curves for single compression of the initial modification, a horizontal plateau where the standard measurement techniques fix a constant velocity D_{crit} of the leading shock wave of the beginning of the transformation, and the Hugoniot adiabatic curve of the second phase after restoration of the single surface of discontinuity. The experimental data relating to the two phases are interpreted as two independent sets described by Eq. (3.1). A more complicated four-term expression given in [46], adequately reflecting the singularities of the phase transitions, was used for iron, since the transformation $Fe_\alpha - Fe_\varepsilon$ is accompanied by a large volume change ΔV.

For four elements with small values of ΔV the principal characteristics of the D(u) curves are shown in Table 12, which differs from Table 11 in that u_{crit} has been replaced by two values for the boundaries of the plateau, $u_{crit.low.}$ and $u_{crit.upp.}$. Let us consider the results obtained for each of the metals, referring to Fig. 9*and Fig. 3. In [28, 59, 14] Ti was regarded as a metal having a smooth adiabatic curve. A slight discontinuity in the data below 1 km/sec, indicating the presence of a phase transition, was discovered in [24], and the components of the new phase in the retained specimens were found in [59]. The description proposed in [24] for the compressibility of Ti does not, however, agree with the measurements (the points 4) of [28] when $u \approx 0.70$ km/sec and with the values (the points 6) for the velocity of sound (4.85-4.95 km/sec) obtained by different methods [35, 38, 41].

The figures also show below the line of the first phase the subsequent verifying shock-wave measurements (the points 1) made by the authors of the present article. The question of the initial segment of the adiabatic curve for Ti still remains undecided. The equation for its second branch, given for the first time in Table 12, satisfactorily describes experiments from 0.9 to 9.4 km/sec, which include measurements on explosive and pneumatic [23] propelling systems. Unlike the case of Ti, in the case of Zr and Hf there is good agreement for all ranges between the results obtained by various authors. The data on Eu were first described [18, 26], as for other lanthanides, by curves of type 4. In [27] the sequence of D, u points for Eu revealed a small plateau at pressures which agreed with the pressures of shock melting (Fig. 11). At large amplitudes of the shock waves the measurements of [19, 26] differed from those of [27] for Eu as well as for Y. The averaging approximation by means of Eqs. (3.1) in this case can be satisfactorily carried out only up to $u \leq 4$ km/sec, although data on the compressibility of Eu are available [26] up to $u = 5.9$ km/sec.

It is of special significance that we obtain the most accurate adiabatic curves for iron, a metal which is used as a standard for the measurements of compressibility at the highest pressures [8-20]. Because of the phase transition $Fe_\alpha - Fe_\varepsilon$, which takes place at 12.8 GPa [60], the D(u) curve for Fe is specifically nonlinear, and, despite the abundance of experimental data, it is known "to within derivatives." In order to take adequate account of the effect of the phase transformation, in [46] the D–u diagram of Fe when $u > u_{crit.low.}$ was found by the following procedure: using the known method of [28], we converted the experimental shock-wave data for the interval $1 < u < 4$ km/sec to a metastable adiabatic curve of the ε phase centered at the density $\rho_{0\varepsilon} = 8.38$ g/cm^3. We assumed that for both phases the Gruneisen coefficients $\gamma = 2/\sqrt{\delta}$, where $\delta = \rho/\rho_0$, $\rho_0 = 7.85$ g/cm^3. The calculated "experimental" points and the results [61, 62] of statistical measurements of the compressibility of the ε phase up to 30 GPa, converted to the shock-compression state, were described, in a manner analogous to the case of Cr, Ni, and Cu, by linear D–u relations. The resulting metastable adiabatic curve

$$D_\varepsilon = 4.853 + 1.434u \tag{3.7}$$

for the inverse recentering to the initial state of the α phase was converted to a relation containing a hyperbolic term

*The notation for the points in Fig. 9c is the same as for Figs. 1-3 and Fig. 7, except for the points 1.

TABLE 13

u	D	p	Δ_D^0	$\left(\frac{\Delta_D^0}{D}\right)_u$, %	$\left(\frac{\Delta_u^0}{u}\right)_p$, %	$\left(\frac{\Delta_p^0}{p}\right)_\delta$, %	$(\Delta_\delta^0)_p \cdot 10^2$
1,0	5,420	42,7	34	0,61	0,27	2,0	0,24
2,0	7,109	111,9	22	0,31	0,11	1,1	0,22
3,0	8,731	206,1	28	0,32	0,10	1,3	0,33
4,0	10,285	323,8	36	0,35	0,10	1,6	0,47
5,0	11,772	463,3	43	0,37	0,09	1,9	0,60
6,0	13,192	622,9	55	0,42	0,09	2,4	0,81
7,0	14,544	801,0	76	0,53	0,10	3,1	1,2
8,0	15,828	996,0	109	0,63	0,12	4,0	1,6
9,0	17,045	1207,0	154	0,90	0,16	6,0	2,5
10,0	18,194	1432	210	1,2	0,19	7,8	3,7

$$D_\alpha = -0.648u^{-1} + 4.547 + 1.462u. \tag{3.8}$$

According to [63], the equation of the low-pressure phase has the form

$$D_u = 4.63 + 1.33u. \tag{3.9}$$

The two branches of the adiabatic curve are joined by a horizontal segment at $D_{crit} = 5{,}060$ km/sec. The left-hand boundary of the plateau ($u_{crit.upp.} = 0.322$ km/sec) corresponds [60] to the beginning of the transformation at 12.8 GPa, the right-hand boundary ($u_{crit.low.} = 0.860$ km/sec) corresponds to the disappearance of the two-wave configuration at 34.0 GPa. Taken together, (3.7)-(3.9) characterize the dynamic compressibility of iron up to pressures of 500 GPa. The region of the phase transition and the initial segment of the upper branch, with a clearly marked nonlinearity, are shown in the lower curve of Fig. 9c.

In order to obtain the analytic form of the entire upper branch of the adiabatic curve for iron up to 1400 GPa, together with its statistical characteristics, we carried out a new quadratic approximation of the experimental data of [28, 29, 32, 24, 20] and Table 1. The result is

$$D_{Fe} = 3.664 \pm 0.065 + (1.79 \pm 0.036)u - (0.0337 \pm 0.00336)u^2. \tag{3.10}$$

In Table 13 we show up to $u \leq 10$ km/sec the confidence intervals Δ_D^0, $(\Delta^0\delta)_p$ corresponding in (3.10) to the values of D, p and the relative confidence intervals $(\Delta^0 u/u)_p$, $(\Delta^0 p/p)\delta$.

The present study generalizes the results of experimental investigations of the dynamic compressibility of 54 metallic elements, obtained up to 1977, as well as results published here for the first time. These measurements, carried out in various ranges of parameters, raised the ceiling of the pressures studied for a number of elements to 1000 GPa, and for iron to 1400 GPa. On the basis of statistical criteria, we give a rational and physically justified classification of shock-wave adiabatic curves on the basis of their configuration in the D–u plane. In addition to two types of curves with singularities caused by the electron transitions (type 4) and phase transitions (type 5), it includes three types of D–u relations of smooth curves with decreasing (type 2) and increasing (type 3) slopes as u increases, as well as with the phenomenon of linearity (type 1), which is mtaintained up to surprisingly large shock-wave amplitudes. A nontrivial feature is the very possibility that simple formulas can be used for the smooth description of completely different states of a metal – for different degrees of compression of the solid phase, shock-wave melting, and intensive heating to temperatures of tens of thousands of degrees.

On the basis of our statistical approach, in addition to the nominal curves, the study also provided us for the first time with the statistical characteristics of the accuracy of their localization on the D–u, p–u, and p–σ diagrams. In particular, it was established that, with a probability of 95%, the possible errors in the pressure values at fixed density do not exceed 2.5% at 400 GPa and 5% at 1000 GPa for Mo, Cu, Ni, and many other metals. These numbers show that even at our present stage of knowledge, the results of the dynamic investigations constitute a promising basis for the metrology of high and super-high pressures.

New conclusions were arrived at in the approximation of nonsmooth curves of shock compression by finding their optimal subdivision into segments. The confidence intervals for the position of the break-points in a number of metals, as evaluated by means of a specially designed algorithm, proved to be unexpectedly large. For Ho, Er, and Tu the indeterminacy in the location of the break-point is now about 20 GPa, while for Gd and Tb it is about 15 GPa. The very concept of the break-point is still formal and approximative in character, and a determination of the physical nature of the transition zone and its actual width will require the use of nontraditional methods for recording the derivatives of the compression curves.

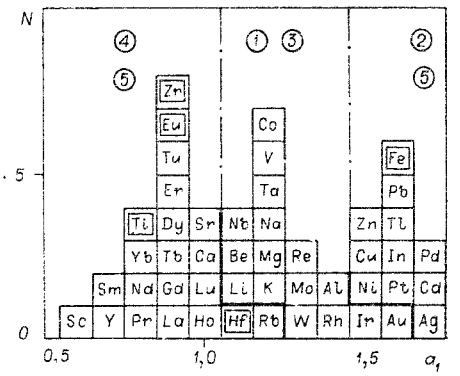

Fig. 12

The approximation coefficients a_0 and a_1 represent essential physical characteristics of the solid. Their values, found here by simultaneous statistical processing of dynamic and static data, determine the most reliable initial values of the elastic moduli $K_S = \rho_0 a_0^2$ and their derivatives $(\partial K_S/\partial p)_S = 4a_1$. The parameter a_1 depends regularly on the position of the elements in Mendeleev's periodic table. Reflecting the physical nature of the processes taking place in the atoms of the metal under compression, this parameter determines which particular type the adiabatic curve belongs to. The histogram of the distribution of elements according to the quantity a_1 (Fig. 12), unlike the analogous histogram first proposed in [64], has three maxima, one for each of its three sections. All the elements of the first section, with a maximum at $a_1 = 0.9$, lie in the first four groups of the expanded periodic table and belong to types 4 and 5. For adiabatic curves of type 4 the anomalously small values of a_1 are explainable by the fact that electrons are shifted to inner orbits under compression. As a result of this process, the "boundary" density of the electrons, the resulting pressure, and the elasticity of the metal remain almost constant. The same processes take place in Ti, Zr, and Hf. In the initial state these metals crystallize in close-packed hexagonal form. The low-compressibility states found in these metals and in Eu are due to the reconstruction of their energy spectra and electron shells.

Centered around the second maximum at $a_1 = 1.2$ we find essentially those elements which do not undergo electron transitions – light alkali and alkaline-earth metals and transition elements from the fifth and sixth groups of the periodic table. Here the types of adiabatic curves are distinguished, on the one hand, by the nearness of a_1 to 1.25, the asymptotic slope of the D(u) functions, and on the other hand by large values of the Gruneisen electron coefficients, which the transition metals may have in the ranges under consideration. Elements in the middle part of the histogram are therefore characterized by adiabatic curves of type 1, which retain the phenomenon of linearity over wide ranges of the parameters, and adiabatic curves of type 3 in the case of elements for which the thermal excitation of the electrons leads to a sharp rise in elasticity (Co, Ta, Nb, V, Rh).

The third sector of the histogram is formed by metals which occupy the right side of Mendeleev's table. The third maximum lies at $a_1 = 1.6$, and the values of a_1 vary in this case over a narrow interval from 1.5 to 1.7. These values are considerably higher than the limiting slopes of the D–u relations for strong shock waves. Therefore a tendency toward a decrease in the derivatives dD/du for specific pressure levels is characteristic of all elements in this section whose adiabatic curves were found to belong to type 2. As the experimentally studied ranges are expanded, this same configuration will probably be found for the shock-compression curves of Al, Ir, and Au.

The authors are deeply grateful to B. M. Stepanov, at whose initiative this study was undertaken. The authors sincerely thank A. V. Bushman, A. N. Dremin, and V. E. Fortov for their help in systematizing the information and A. L. Velikovich for his part in the development of the statistical algorithms.

LITERATURE CITED

1. L. V. Al'tshuler, "Use of shock waves in high-pressure physics," Usp. Fiz. Nauk, 85, No. 2 (1965).
2. Ya. B. Zel'dovich and Yu. P. Raizer, Physics of Shock Waves and High-Temperature Hydrodynamic Pressures [in Russian], Fizmatgiz, Moscow (1963).
3. P. Caldirola and H. Knoepfel (editors), Physics of High-Energy Density, Academic Press, New York (1971).
4. V. Zharkov and V. A. Kalinin, Equations of State of Solids at High Pressures and Temperatures [in Russian], Nauka, Moscow (1968).

5. H. K. Mao et al. "Specific volume measurements of Cu, Mo, Pd, and Ag and calibration of the ruby fluorescence pressure gauge from 0.06 to 1 Mbar," J. Appl. Phys., 49, No. 6 (1978).
6. Ragan et al., "Shock compression of molybdenum to 2.0 TPa by means of nuclear explosion," J. Appl. Phys., 48, No. 7 (1977).
7. L. V. Al'tshuler and A. A. Bakanova, "Electronic structure and compressibility of metals at high pressures," Usp. Fiz. Nauk, 96, No. 2 (1968).
8. L. V. Al'tshuler, K. K. Krupnikov, and M. K. Brazhnik, "Dynamic compressibility of metals at pressures from 4000 to 4,000,000 atm," Zh. Eksp. Tekh. Fiz., 34, No. 4 (1958).
9. L. V. Al'tshuler et al., "Dynamic compressibility and equation of state of iron at high pressures," Zh. Eksp. Tekh. Fiz., 34, No. 4 (1958).
10. L. V. Al'tshuler et al., "Equations of state of aluminum, copper, and lead for the region of high pressures," Zh. Eksp. Tekh. Fiz., 38, No. 3 (1960).
11. L. V. Al'tshuler, A. A. Bakanova, and R. F. Trunin, "Shock-wave adiabatic curves and zero isotherms of seven metals at high pressures," Zh. Eksp. Tekh. Fiz., 42, No. 1 (1962).
12. K. K. Krupnikov et al., "Shock-wave compression of porous tungsten," Zh. Eksp. Tekh. Fiz., 42, No. 3 (1962).
13. S. B. Kormer et al., "Dynamic compression of porous metals and equations of state with variable heat capacity at high temperatures," Zh. Eksp. Tekh. Fiz., 42, No. 3 (1962).
14. K. K. Krupnikov et al., "Investigation of shock compressibility of titanium, molybdenum, tantalum, and iron," Dokl. Akad. Nauk SSSR, 148, No. 6 (1963).
15. A. A. Bakanova, I. P. Dudoladov, and R. F. Trunin, "Compression of alkali metals by strong shock waves," Fiz. Tverd. Tela, 7, No. 6 (1965).
16. L. V. Al'tshuler, A. A. Bakanova, and I. P. Dudoladov, "Characteristics of the shock compression of lanthanides," Pis'ma Zh. Eksp. Tekh. Fiz., 3, No. 12 (1966).
17. A. A. Bakanova and I. P. Dudoladov, "Compression of alkaline-earth metals by strong shock waves," Pis'ma Zh. Eksp. Tekh. Fiz., 5, No. 9 (1967).
18. A. A. Bakanova, I. P. Dudoladov, and Yu. N. Sutulov, "Electron transitions in hafnium, europium, and ytterbium at high pressures," Fiz. Tverd. Tela, 11, No. 7 (1969).
19. L. V. Al'tshuler A. A. Bakanova, and I. P. Dudoladov, "The effect of electron structure on the compressibility of metals at high pressures," Zh. Eksp. Tekh. Fiz., 53, No. 6 (1967).
20. L. V. Al'tshuler and B. F. Chekin, "Metrology of pulsed pressures," in: Reports of the First All-Union Symposium on Pulsed Pressures [in Russian], VNIIFTRI, Moscow (1974).
21. A. H. Jones et al., "Measurement of the very-high-pressure properties of materials using a light-gas gun," J. Appl. Phys., 37, No. 9 (1966).
22. J. A. Morgan, "The equation of state of platinum to 680 GPa," High Temp.-High Pres., 6, No. 2 (1974).
23. M. Van Thiel, Compendium of Shock-Wave Data, Vol. 1, UCRL 50108 (1977).
24. R. McQueen et al., in: High-Velocity Impact Phenomena, R. Kinslow (editor), Academic Press, New York–London (1970).
25. R. Duff et al., in: The Behavior of Dense Media under High Dynamic Pressure, Gordon and Breach, New York (1968).
26. W. Gust and H. Royce, "New electronic interaction in rare-earth metals at high pressure," Phys. Rev., B8, No. 8 (1973).
27. W. J. Carter et al., "Hugoniot equation of state of the lanthanides," J. Phys. Chem. Solids, 36, Nos. 7-8 (1975).
28. M. H. Rice, R. G. McQueen, and J. M. Walsh, in: Solid State Physics, F. Seitz and D. Turnbull (editors), Vol. 6, Academic Press, New York–London (1958).
29. R. G. McQueen and S. P. Marsh, "Equation of state for nineteen metallic elements," J. Appl. Phys., 31, No. 7 (1960).
30. M. H. Rice, "Pressure–volume relations for the alkali metals from shock-wave measurements," J. Phys. Chem. Solids, 26, No. 3 (1965).
31. M. Van Thiel and A. S. Kusubov, Compendium of Shock Wave Data, Vol. 1, NBS, Springfield (1966).
32. J. S. Skidmore and E. Morris, Thermodynamics of Nuclear Materials, Vienna (1962).
33. D. P. Dandekar, "Loss of shear strength in polycrystalline tungsten under shock compression," J. Appl. Phys., 47, No. 10 (1976).
34. A. N. Dremin and K. I. Kanel', "Compression and rarefaction waves in shock-compressed metals," Zh. Prikl. Mekh. Tekh. Fiz., No. 2 (1976).
35. K. A. Gshneidner, in: Solid State Physics, F. Seitz and D. Turnbull (editors), Vol. 16, Academic Press, New York–London (1964).

36. S. N. Vaidya and G. C. Kennedy, "Compressibility of 18 metals to 45 kbar," J. Phys. Chem. Solids, 31, No. 10 (1970).
37. S. N. Vaidya and G. C. Kennedy, "The compression of the alkali metals to 45 kbar," J. Phys. Chem. Solids, 32, No. 11 (1971).
38. S. N. Vaidya and G. C. Kennedy, "Compressibility of 22 elemental solids to 45 kbar," J. Phys. Chem. Solids, 33, No. 7 (1972).
39. L. C. Ming and M. H. Manghnam, "Isothermal compression of bcc transition metals to 100 kbar," J. Appl. Phys., 49, No. 1 (1978).
40. O. L. Anderson, in: Physical Acoustics, W. R. Mason (editor), Vol. 3B, Academic Press, New York–London (1965).
41. M. W. Guinan and D. J. Stenberg, "Pressure and temperature derivatives of the isotropic polycrystalline shear modulus for 65 elements," J. Phys. Chem. Solids, 35, No. 11 (1974).
42. A. L. Ruoff, "Linear shock-velocity–particle-velocity relationships," J. Appl. Phys., 38, No. 13 (1974).
43. D. J. Pastine and D. Piacesi, "The existence and implications of curvature in the relation between shock and particle velocity for metals," J. Phys. Chem. Solids, 27, No. 8 (1966).
44. B. Alder, in: Solids under Pressure, W. Paul and D. Warchaur (editors), McGraw-Hill, New York (1963).
45. A. I. Voropinov, G. M. Gandel'man and V. G. Podval'nyi, "Electron energy spectra and equations of state of solids at high pressures and temperatures," Usp. Fiz. Nauk, 100, No. 2 (1970).
46. L. V. Al'tshuler and B. S. Chekin, "Relaxation parameters of metals behind shock-wave fronts," in: Detonation. Critical Phenomena. Physical and Technical Transformations in Shock Waves [in Russian], OIKhF, Chernogolovka (1978).
47. V. N. Tutubalin, Theory of Probability [in Russian], Nauka, Moscow (1972).
48. N. P. Klepikov and S. N. Sokolov, Analysis and Planning of Experiments by the Method of Maximum Probability [in Russian], Nauka, Moscow (1964).
49. D. J. Hudson, Statistics, Geneva (1964).
50. F. E. Prieto and C. Renero, "Equation of state of solids," J. Phys. Chem. Solids, 37, No. 1 (1976).
51. B. S. Chekin, "Dimensionless equations of state and attenuation of shock waves," Zh. Prikl. Mekh. Tekh. Fiz. No. 2 (1978).
52. F. E. Prieto and C. Renero, "Equation of shock adiabat," J. Appl. Phys., 41, No. 9 (1970).
53. R. Grover, "Comments on the comparison of dynamic and static compression data," J. Phys. Chem. Solids, 31, No. 10 (1970).
54. E. Yu. Tonkov, Phase Diagrams of Elements at High Pressure [in Russian], Nauka, Moscow (1979).
55. R. Grover and B. J. Alder, "Absence of first order electronic transitions in liquid metals," J. Phys. Chem., 35, No. 7 (1974).
56. L. V. Al'tshuler et al., "Isentropic compressibility of aluminum, copper, lead, and iron at high pressures," Zh. Eksp. Tekh. Fiz., 38, No. 4 (1960).
57. E. M. Savitskii et al., Alloys of Rare-Earth Metals [in Russian], Akad. Nauk SSSR, Moscow (1962).
58. J. W. McCaffrey, "Band structure and pressure-induced electronic transitions in calcium," Sol. State Commun., 8, No. 24 (1970).
59. A. R. Kutsar and V. I. German, "Study of the structure of titanium after processing by shock waves," in: Titanium. Metallurgy and Technology [in Russian], VILS, Moscow (1978).
60. G. E. Duvall and R. A. Gracham, "Phase transformation under shock-wave loading," Rev. Mod. Phys., 49, No. 3 (1977).
61. T. Takanashi et al., "Isothermal compression of the alloys of iron up to 300 kbar at room temperature: iron–nickel alloys," J. Geophys. Res., 73, No. 14 (1968).
62. P. M. Giles et al., "High-pressure $\alpha \rightleftharpoons \varepsilon$ martensite transformation in iron," J. Appl. Phys., 42, No. 11 (1971).
63. L. M. Barcer, "α-Phase Hugoniot of iron," J. Appl. Phys., 46, No. 6 (1975).
64. V. F. Anisichkin, "Generalized adiabatic curves of elements," Zh. Prikl. Mekh. Tekh. Fiz., No. 3 (1978).